

ARTICLE

Constitutive model for plain and fiber-reinforced lightweight concrete under compression

Hasanain K. Al-Naimi | Ali A. Abbas 

University of East London, London, UK

CorrespondenceAli A. Abbas, University of East London,
London, UK.Email: abbas@uel.ac.uk**Abstract**

In this research work, experimental investigations of the compressive behavior of plain and fiber-reinforced lightweight-aggregate concrete have been carried out (this formed part of a wider study, which also examined tensile and flexural behaviors). Compression mechanical properties were established in the studies and a generic constitutive compressive σ - ϵ model for both plain and fibrous lightweight concrete was derived and validated against experimental results from the present studies and previous research in the literature involving different types of lightweight aggregates, concrete strengths, and steel fibers. The reliability of predictions of the constitutive model was also checked against existing fibrous concrete models. A fiber-reinforcing factor was also introduced taking into account the fiber volume fraction, fiber length and diameter, the number of fiber bends, and concrete compressive strength. As such, this was considered a better descriptor of the material than simply using the fiber volume fraction. The lightweight aggregates examined in the experimental study were recycled from fly ash waste and the fibers were hooked-ended with single, double, and triple bends (corresponding to DRAMIX steel fibers 3D, 4D, and 5D types, respectively). The fibers were added at volume fractions V_f of 1% and 2% and the experimental studies were carried out using standard cube and cylinder uniaxial compression test specimens. It was concluded that the higher the number of bends and fiber content, the more pronounced the enhancement provided by the fibers to the compressive strength and ductility responses. All steel fibers used in the present studies were found to significantly improve the compressive toughness, while only 4D and 5D fibers (i.e., those with double and triple end bends) enhanced the compressive strength by up to 12% and 15%, respectively. It was also found that the elastic properties of plain lightweight concrete remained unaffected by the addition of fibers.

KEYWORDScompressive strength, compressive toughness, constitutive compressive σ - ϵ model, ductility, hooked-end steel fibers, lightweight concrete

This is an open access article under the terms of the [Creative Commons Attribution](https://creativecommons.org/licenses/by/4.0/) License, which permits use, distribution and reproduction in any medium, provided the original work is properly cited.

© 2023 The Authors. *Structural Concrete* published by John Wiley & Sons Ltd on behalf of International Federation for Structural Concrete.

1 | INTRODUCTION

The use of structural lightweight aggregate concrete (LWAC) as a replacement to conventional normal-weight aggregate concrete (NWAC) is essentially aimed at decreasing gravity and inertial loads and increasing the strength-to-weight ratio.¹ This in turn leads to a reduction in cross-sectional sizes required for key elements such as columns, beams, slabs, and foundations and an increase in building space,² which promotes overall savings in materials, transport costs, and construction time. This has environmental benefits. In addition, the porous nature of LWAC brings several other advantages such as increased thermal insulation, noise absorption, and fire resistance.^{3,4} Besides, the lightweight aggregate used in the present experimental investigations is from recycled waste and thus offers further reduction in CO₂ emissions as well as being an alternative to the depleting gravel and quarried natural resources.⁵ The lightweight aggregates used are recycled fly ash waste (commercially known as LYTAG), which is a by-product of coal-fired electricity power stations.⁶ Fly ash, also termed Pulverized Fuel Ash (PFA), is the ash resulting from the burning of pulverized coal in these power stations. A study on LYTAG in 2014 showed that it can bring about 34% savings in CO₂ with reduction of up to 48% of concrete and reinforcement when compared to conventional gravel concrete.⁷ The usage of lightweight concrete is thus needed in the construction industry due to the growing need for sustainable designs for taller and longer span structures, especially in seismic zones.^{8–11} Modern structural applications of LWAC also include bridges and towers. However, these advantages are tempered by the increased brittleness of lightweight concrete. The latter is thought to be the product of the more porous concrete matrix and poorer aggregate interlock mechanism in LWAC as compared to NWAC, which translates into lack of natural toughening mechanism post-crack.⁵ On the material level, this causes somewhat more pronounced failures in both compression and tension, while on the structural level, LWAC exhibits reduced shear capacity and excessive deflection and cracking due to the lower modulus of elasticity.^{12–15} Structural PFA-LWAC (i.e., LYTAG) has been around since the 1960s; however, limited comprehensive research has been carried out on its mechanical properties.^{16,17} Moreover, equations to define the material and structural properties of LWAC are usually adapted from studies in the last century based on NWC.^{13,15,18,19}

The brittle nature of lightweight concrete can be addressed normally by incorporating traditional steel reinforcement. However, the latter solution can become increasingly impractical when reduction in structural element sizes is sought by employing LWAC, especially at critical zones such as joints. Therefore, steel fiber

reinforcement, which has proven its effectiveness in increasing ductility of several fibrous composites in the past, can become an adequate solution for brittle LWAC.^{20–24} The earliest work examining the advantages of the usage of steel fibers in lightweight concrete have been reported several years ago.²⁵ Nonetheless, the application of steel fiber reinforcement in lightweight concrete is still largely in the development phase with most of the current work being merely theoretical and carried out at the structural level only (with little focus on the fundamental material behavior) and involving different lightweight aggregates such as pumice stone and oil palm aggregates.^{23,24,26–28} Thus, the present comprehensive experimental investigations of fibrous recycled LWAC are beneficial for the rapidly developing concrete technology, since coal-fired power generation remains the largest contributor of energy in the world.²⁹ Furthermore, it should be noted that, at present, there is no international standards specific for steel fiber-reinforced lightweight concrete (SFRLC) with current guidelines being usually adapted from their steel fiber-reinforced *normal-weight* concrete (SFRC) counterparts. So the findings of the present research study will help provide an insight into the structural responses of SFRLC and proposing a semi-empirical constitutive model to predict the compressive stresses and strains of both LWAC and SFRLC. The research also serves to quantify the influence of multiple bend fibers on the pre- and post-peak compressive behavior of fibrous concrete.

2 | LITERATURE REVIEW

It is well established that the addition of steel fibers enhances the flexural behavior of lightweight concrete.^{2,8,20,24,26,28,30–33} However, some disparity in results were reported concerning the influence of steel fiber reinforcement on the compressive behavior of lightweight concrete. This can be due to the different parameters inspected such as the target compressive strength, aggregate type, steel fiber type, its geometry, shape, and content. Some researchers who carried out compressive tests on SFRLC reported a negative influence on the compressive strength and modulus of elasticity and a positive influence on the compressive ductility as compared to plain LWAC. For instance, an experimental study on expanded clay lightweight concrete reinforced with straight micro steel fibers with volume fraction $V_f \leq 1.25\%$ in compression, reported a maximum decrease of 12% in compressive strength.²⁸ Similarly, another study measured a decrease of 15% in the compressive strength of expanded clay lightweight concrete reinforced with hooked-end steel fibers with $V_f \leq 0.5\%$.²⁴ In addition, compressive tests were

carried out on oil palm shell lightweight concrete reinforced with hooked-end steel fibers and found a decrease in compressive strength of 6.7% when $V_f > 0.5\%$, and an increase of 6% when $V_f < 0.5\%$.¹¹ Finally, tests on shale ceramic reinforced with steel fibers with $V_f \leq 0.9\%$, revealed that a maximum decrease of compressive strength of 18%.² Some researchers blamed the decrease in compressive strength of SFRLC on the reduction in fibrous specimens density caused by the presence of air voids due to the addition of fibers, especially noticeable when $V_f > 0.5\%$.^{11,24} On the other hand, some researchers observed an increase in both the compressive strength and ductility of expanded clay lightweight concrete as the fiber content was increased, while pumice lightweight concrete exhibited a reduction in compressive strength and increase in ductility as fiber content was increased.³⁴ In the study,³⁴ the differences in the behavior of both types of lightweight concrete were attributed to the fiber length to maximum aggregate size ratio, which was lower and hence more favorable for the expanded clay aggregate as compared to the pumice aggregate. The aggregate size and type from different literature were used to validate findings of the present research. Similar to the expanded clay concrete responses reported in,³⁴ another study found an increase in compressive strength and ductility of oil palm shell concrete (OPSC) as fibers were added.³¹ They reported beneficial impact of steel fiber reinforcement on lightweight concrete, however, seems to be varied. For instance, several researchers reported an increase of up to about 20% ~ 32% in lightweight concrete compressive strength with the addition of steel fibers with dosages of up to 2%.^{20,34-38} Other researchers reported a drastic increase in compressive strength of lightweight concrete of up to 61% ~ 72% with steel fiber reinforcement volume fractions of up to 2%.^{8,32,33} Generally, no detailed explanation was provided as to why steel fibers result in an increase in compressive strength, and merely observations were reported. The present research work will attempt to provide explanation to such behavior in Section 4. It was found that the increase in compressive strength is due to the activation of the fiber confinement effect on the concrete specimen, as the fibers bridge the lateral crack developing due to tension in the orthogonal direction. Moreover, it was observed that the effect of steel fiber reinforcement on compressive strength became more prominent as the lightweight aggregate content was increased.^{39,40} Scarce research was found on fibrous recycled fly-ash based LWAC such as LYTAG; so for instance, the latter was tested with $V_f \leq 1\%$ and found no particular pattern in relation to the compression strength when fibrous and plain lightweight concrete were compared.^{26,41,42} Further testing was also carried out to examine the effect of polypropylene (provided at a volume fraction $V_f = 0.56\%$) and steel (at $V_f = 1.7\%$) fibers on LYTAG fly-

ash based high strength lightweight aggregate concrete and it was reported that a reduction in compressive strength of up to 11% was observed.³⁰ Given the scatter in the results of SFRLC reported herein, there is an urgent need for further investigations on the compression behavior of SFRLC, particularly steel fiber-reinforced fly-ash based lightweight concrete. This work serves to offer more clarity and understanding on this key fundamental material behavior. The present experimental studies also culminate in deriving a compressive constitutive σ - ϵ model for SFRLC based on different hooked-end steel fiber types, geometries, contents, and plain concrete compressive strengths. Validation of the proposed model using experimental tests performed in the present studies as well as those found in the literature is also carried out.

There are different types of steel fibers including both engineered and natural/recycled ones. There is currently a rapid increase in the development of concrete utilizing different waste fibers due to potential economic and environmental benefits.⁴³ Several studies were reviewed by Kalpana and Tayu⁴³ examining waste steel from steel reinforcement and formworks, which were mixed with structural light-weight concrete incorporating various fiber contents and this has resulted in preventing brittle failure in lightweight concrete. Improvements to strength were also reported, which were linked to optimum fiber dosages. Karalar et al.⁴⁴ experimentally examined beams with different amounts of longitudinal reinforcement and volume fractions of waste lathe scraps ranging from 1% to 3% and reported improvement in bending performance and also in compressive strength. Similar results were also reported on a study by Elik et al.⁴⁵ investigating the performance assessment of fiber-reinforced concrete produced with waste lathe fibers. Zeybek et al.⁴⁶ carried out experimental investigations to evaluate the performance of concrete reinforced with steel fibers extracted from waste tires with volume fractions 1%, 2%, and 3% (with compression, splitting tensile, and flexure tests carried out). It was found that the mechanical properties were improved with the addition of fibers; however, workability was significantly reduced with the addition of more than 2% volume fraction of fibers. Furthermore, empirical equations were developed to predict the compressive and splitting tensile strengths and strains. Limited experimental studies were carried out on lightweight concrete reinforced with steel fibers with multiple end hooks (i.e., 4D and 5D fibers), despite their increased use in normal weight concrete applications. Dehghani and Aslani⁴⁷ experimentally examined the effect of 3D, 4D, and 5D hooked-end type on the pull-out behavior of fibers embedded in cementitious composites and it was found that the use of more bends at hooked-end (i.e., 5D vs. 3D) significantly enhances the bond strength of fibers. Guler

and Funda⁴⁸ carried out experimental work to examine the compressive and flexural strengths and toughness capacities of 3D, 4D, and 5D fibers under high temperatures and it was found that these capacities reduced significantly as temperature increased. Mohamed et al.⁴⁹ carried out a comprehensive review of research on the performance of steel fiber-reinforced lightweight concrete. It was found that the load-carrying capacity of SFRLC is increased by the addition of steel fibers, which also limits the spread of cracks and reduces their width. It was also concluded that, by making the concrete lighter, it is possible to provide economical solutions while limiting its deformation.

3 | EXPERIMENTAL PROGRAM

3.1 | Material properties

3.1.1 | Cement

General purpose Portland-limestone cement CEM II was used as the binder according to the specifications supplied in EN 197-1⁵⁰ and EN 196-1.⁵¹

3.1.2 | Aggregate

LYTAG recycled sintered pulverized fly ash aggregates were used as the coarse aggregate of the lightweight concrete in the present experimental study. LYTAG aggregates (4–14 mm) are brown, roughly spherical with a honeycomb structure of interconnected voids, and sometimes irregular in shape as can be seen in Figure 1. LYTAG is fire resistant and highly stable at elevated temperatures with a specific gravity of about 1.8 and water absorption of up to 15%. Furthermore, LYTAG void ratio of about 40% makes it ideal in freeze and thaw conditions. Natural sharp sand with a maximum aggregate size of 4.75 mm was used as the fine aggregate of the concrete. The sand had a water absorption of 0.09% and specific gravity of 2.65 complying with BS EN 12620.⁵² Sieve analysis for both LYTAG and sand can be found in Figure 2. The percentage passing through 600 μm of fine aggregate was found to be 51.2% in the sieve analysis.

3.1.3 | Fibers

DRAMIX hooked-end steel fibers with single-bend (3D), double-bend (4D), and triple-bend (5D) were used in the present experimental study.⁵³ The fibers were essentially



FIGURE 1 Coarse LYTAG aggregate.

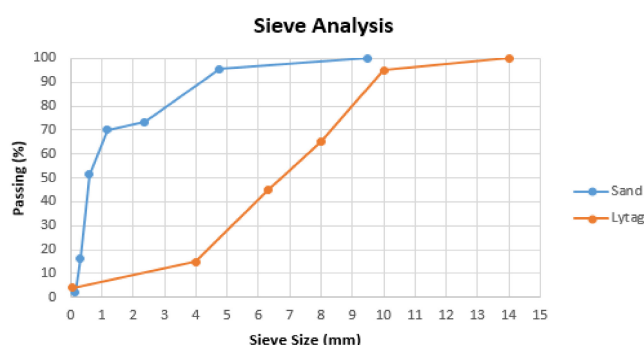


FIGURE 2 Sieve analysis for sand and LYTAG aggregates.

used to address the brittleness of lightweight aggregates and as conventional reinforcement replacement. It has been estimated that two thirds of the fibers used in the industry are hooked-end 3D steel fibers.⁵⁴ For this reason, hooked-end 3D fibers were regarded as the control fibers during the experimental program, while the rest of the fibers were used for the purpose of evaluating the effects of different fiber geometries on the behavior of lightweight concrete. The three fiber types considered in the present experimental program are shown in Figure 3. The modulus of elasticity of these steel fibers is 210 GPa, while the tensile strength varies.⁵⁵ The precise geometrical properties of the fibers and their hooks are illustrated in Table 1, which is adapted from Abdallah et al.^{54,55} who electronically scanned identical fibers and processed the geometrical properties of the hooks using a computer software. The definitions of symbols L1, L2, L3, L4, $\theta 1$, and $\theta 2$ in Table 1 are shown in Figure 4. In order to

prevent the possibility of fibers balling during mixing, DRAMIX fibers were supplied collated together with a type of water dissolvable glue from the manufacturer. Collation was successful at reducing the possibility of fibers balling, thus allowing better fiber dispersion (in a similar manner to that reported by Balaguru and Foden³⁶). The comparison between the performance of these fibers offered an understanding of the

contribution of extensive mechanical anchorage systems (hooks) on the compressive strengths and ductility of SFRLC.

3.2 | Mix proportions

A total of four mixes were cast with the design proportions shown in Table 2. These were adopted from LYTAG manuals⁶ and the extensive experimental studies by Lambert.¹⁶ The quantity of fibers was calculated to be 78.5 and 157 kg per 1 m³ of lightweight concrete for fiber contents of $V_f = 1$ and 2%, respectively. It was opted not to use any superplasticisers or water reducers since the w/c of the mixes was relatively high, while fiber dosage was generally low ($V_f < 2\%$). This further avoids adding an extra variable or limitation to the study. It is important to note that the quantities in Table 2 were increased by a factor of 15% upon mixing to account for any possible freshly mixed concrete losses during workability tests, casting, leveling, and vibration. Based on the mix designs provided by the manufacturer,⁶ as the concrete target strength is increased, the quantity of sand is reduced, while that of cement is increased. The calculated dry density expected was around 1800 kg/m³. It should be noted that LYTAG mix design manual⁶ recommends an effective water quantity of 180 kg/m³; however, it was observed that this quantity contributes to an overly workable mix. Hence, it was suggested that the effective water was reduced to 175 kg/m³, which also agrees with recommendations from Lambert.¹⁶



FIGURE 3 Fibers used in this work.

TABLE 1 Properties of hooked-end fibers used⁵³ and geometrical properties of hooks are adapted from Abdallah et al.^{54,55}

Fiber type	σ_u (MPa)	σ_y (MPa)	L_f (mm)	d_f (mm)	L1 (mm)	L2 (mm)	L3 (mm)	L4 (mm)	Θ_1 (°)	Θ_2 (°)
3D	1160	775–985	60	0.9	2.12	2.95	–	–	45.7	–
4D	1500	1020–1166	60	0.9	2.98	2.62	3.05	–	30.1	30.8
5D	2300	1177–1455	60	0.9	2.57	2.38	2.57	2.56	27.9	28.2

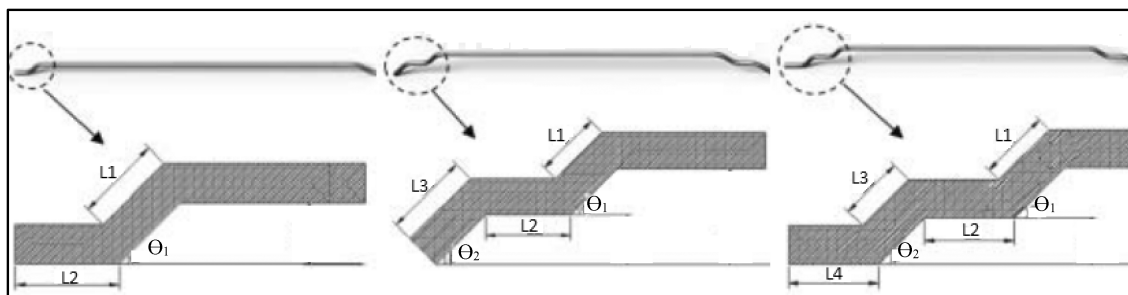


FIGURE 4 Definition of fiber parameters used in Table 1 for 3D, 4D, and 5D fibers (adapted from Bekaert⁵³).

TABLE 2 Design of the four different mixes used in the experimental studies.

Mix	V _f (%)	Fiber	f _{ick} /f _{ick,cube}	Cement (kg/m ³)	Sand (kg/m ³)	LYTAG (kg/m ³)	Effective water (kg/m ³)
1	0, 1, 2	3D	LC30/33	370	592	635.6	175
2		4D					
3		3D	LC35/38	420	546		
4		5D	LC40/44	480	485		

TABLE 3 Average densities, water content, and absorption of LYTAG aggregates.

Air dry loose density of LYTAG in lab conditions (kg/m ³)	757.12 (13)
Oven dry loose bulk density of LYTAG (kg/m ³)	722.28 (12.8)
Saturated surface dry loose density of LYTAG (kg/m ³)	842.31 (15.54)
Water content in aggregate per mass of LYTAG in Lab (%)	4.62 (0.36)
Maximum water absorption per mass of LYTAG (%)	14.3 (0.76)

Note: Standard deviation values are shown between brackets.

3.3 | Specimen preparation

Average values for air dry, oven dry, and saturated surface dry (SSD) loose densities, along with those for the water content and maximum water absorption for LYTAG aggregates, were measured in the laboratory using 10 samples (Table 3). Measuring the water content of LYTAG was of utmost importance as LYTAG aggregates were found to absorb water of approximately 15% of their weight, which also agrees with LYTAG manual.⁶ Water absorption was determined based on BS EN 1097-6:2013.⁵⁶ For this reason, LYTAG aggregates were completely submerged in water for 24 h prior to mixing to ensure maximum water absorption of the aggregates. On the day of mixing, LYTAG aggregates were then taken out of the water and surface dried for 10 min using a dry towel to achieve SSD state, then directly added to the mix. This is considered to be an effective way to achieve SSD as revealed in previous studies.⁵⁷ This method guaranteed that the fresh concrete was workable at all stages, the compressive strength adequate, and surface finishing satisfactory. Sand was oven-dried for 1 day at 100°C prior to mixing. It should be noted that a preliminary study requiring aggregates to be submerged in water 30 min before mixing with an effective water of 180 kg/m³ as suggested by Lyag⁶ resulted in overly high slump values and difficulty in finishing.^{57,58} The materials were mixed in a power-driven rotatory mixer with a capacity of 75 L using recommendations from the lightweight aggregate manufacturer's manual

(Figure 5). Following mixing, the concrete was poured in molds in 3–5 layers depending on the size of the specimen and fiber content. Depending on the volume of the mix and its water/cement ratio, the time taken to vibrate the specimens varied from one mix to another, although good quality was ensured for surface finishing and even distribution of coarse LYTAG aggregates throughout the casting process. After casting, the specimens were wrapped with plastic sheets to prevent water evaporation and left in the concrete laboratory for 24 h at a temperature of 20 ± 2°C and humidity of 50 ± 5%. Finally, the specimens were demolded and cured in a water tank for 28 days prior to mechanical testing in accordance with BS EN 12390-2.⁵⁹

3.4 | Test methods

This work highlights crushing cube tests and uniaxial compression cylinder tests. Each mix included three repeated specimens per V_f for both cubes and cylinders. This led to a total of nine cubes and nine cylinders per mix. Cylinders with height of 200 mm and diameter of 100 mm were used, while the cubes tested had a width of 100 mm.

3.4.1 | Compressive crushing cube test

In the present experimental studies, compressive crushing cube tests were an indicative of the consistency and quality of the mix design. These quick and simple tests were carried out (Figure 6) to directly measure the crushing strength of plain and fibrous lightweight concrete at 28 days. The loading rate used for these tests was 2.3 kN/s according to C39/C39M.⁶⁰

3.4.2 | Uniaxial compression cylinder test

Due to their uniform stress distribution, cylinders were chosen to evaluate the complete compressive stress-strain behavior of LWAC and SFRLC, including static modulus of elasticity and Poisson's ratio. A calibrated compressometer–extensometer steel ring designed according to ASTM C 469⁶¹ was clamped onto the concrete

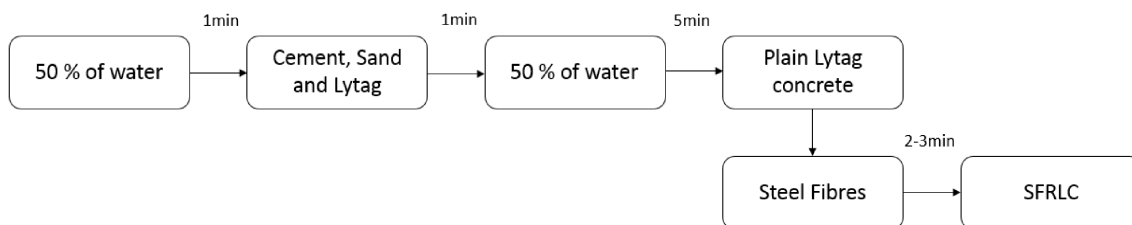


FIGURE 5 Mixing process for plain and fibrous lightweight concrete.



FIGURE 6 Crushing cube test.

cylinders as shown in Figure 7. The compressometer consisted of two yokes. The top one was free to rotate as it was pinned in two opposite points aligned with the center of the cylinder, while the bottom one was fully attached onto the cylinder using three bolts in a way that a straight line passing through a bolt and the center of the cylinder made an angle of 120° with the line passing through the neighboring bolt and the center of the cylinder. A pivot rod was used to maintain a constant distance between the two compressometer yokes. At mid-height of the cylinder, there was a relaxed Linear Variable Differential Transformer (LVDT), which measured the vertical displacement of the specimen. To calculate the vertical deformation based on Figure 8, the following formula was used:

$$d = ge_r / (e_r + e_g)$$

where d , g , e_r , and e_g are the total deformation of the specimen (measured in mm), vertical LVDT gauge reading (measured in mm), the perpendicular distance between the clamped point of the rotating yoke and location of the pivot, and the perpendicular distance between the gauge and clamped point of the rotating yoke, respectively. Since distances e_r and e_g were set to be equal then:

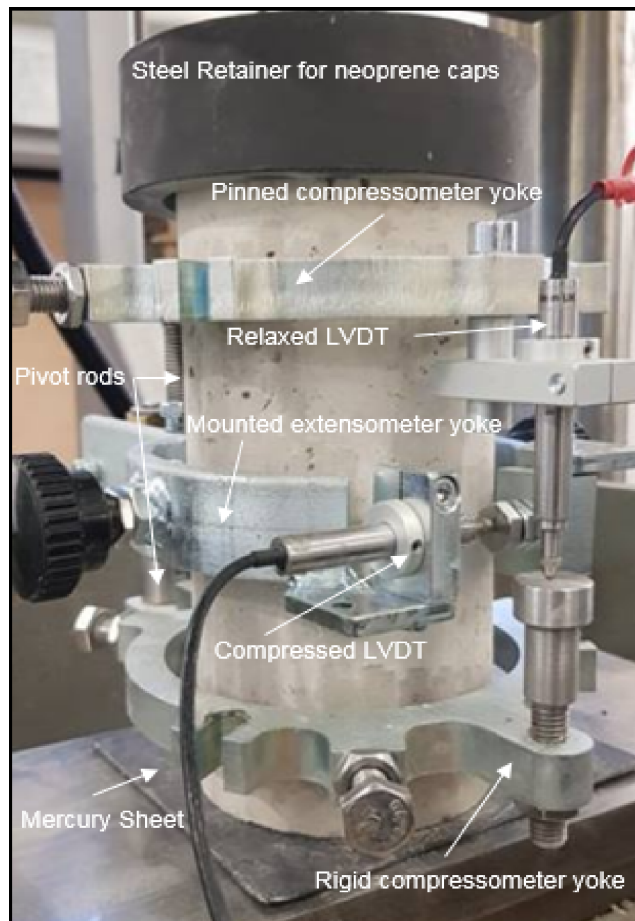
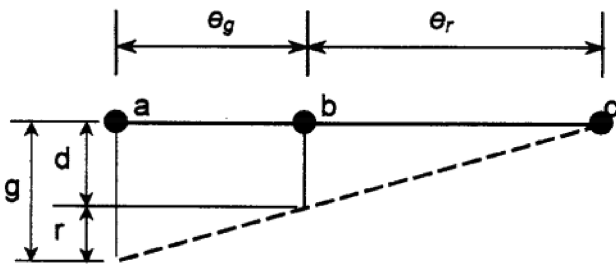


FIGURE 7 Compressometer–extensometer steel ring.

$$d = g/2$$

As shown in Figure 7, an extensometer was mounted circumferentially at opposite points. A pivot rod was also provided to maintain a constant distance between the bottom and middle yokes. The extensometer yoke was open in a way to allow an initially fully compressed LVDT at the middle height of the cylinder to be set up. This LVDT measured the transverse deformation.

By adopting a similar diagram to the one shown in Figure 7, the transverse deformation of the diameter can be calculated using:



d = displacement due to specimen deformation
 r = displacement due to rotation of the yoke about the pivot rod
 a = location of gauge
 b = support point of the rotating yoke
 c = location of pivot rod
 g = gauge reading

FIGURE 8 Calculation of deformations (adapted from ASTM C469⁵⁵).

$$d' = g'/2$$

where d' and g' are the transverse deformation of the specimen diameter (mm) and the transverse LVDT gauge reading (mm), respectively.

To calculate the modulus of elasticity⁶¹:

$$E = (S_2 - S_1) / (\varepsilon_2 - \varepsilon_1)$$

where S_1 , S_2 , ε_1 , and ε_2 are the stress at ε_1 (MPa), the stress at 40% of peak load (MPa), the strain of 0.000050 and the longitudinal strain at S_2 , respectively.

To calculate Poisson's ratio⁶¹:

$$\mu = (\varepsilon_{t2} - \varepsilon_{t1}) / (\varepsilon_2 - \varepsilon_1)$$

where ε_{t2} and ε_{t1} are the mid-height transversal strains at S_2 and S_1 , respectively.

The exact placement of the compressometer-extensometer ring along the height of the cylinder is shown in Figure 9. Before testing, a neoprene pad with a steel retainer was used according to ASTM C1231/C1231M⁶² to cap the cylinders and ensure a uniform distribution of the load at the uneven top surface of the cylinders. The neoprene capping method brought several advantages when compared to the classic sulfur capping method such as time saving in preparation of specimen, reduction in cost and safety of engineer and environment.⁶³ In addition, unbounded neoprene capping does not alter the strength at the top surface of the concrete in comparison with other types of capping (such as sulfur and gypsum capping) provided that the correct hardness of the neoprene cap is chosen. In this work, neoprene pads of 60 shore hardness for strengths ranging between 10 and 48 MPa were used. Moreover, the caps can be applied easily and immediately unlike in the case for the common capping compounds, which also

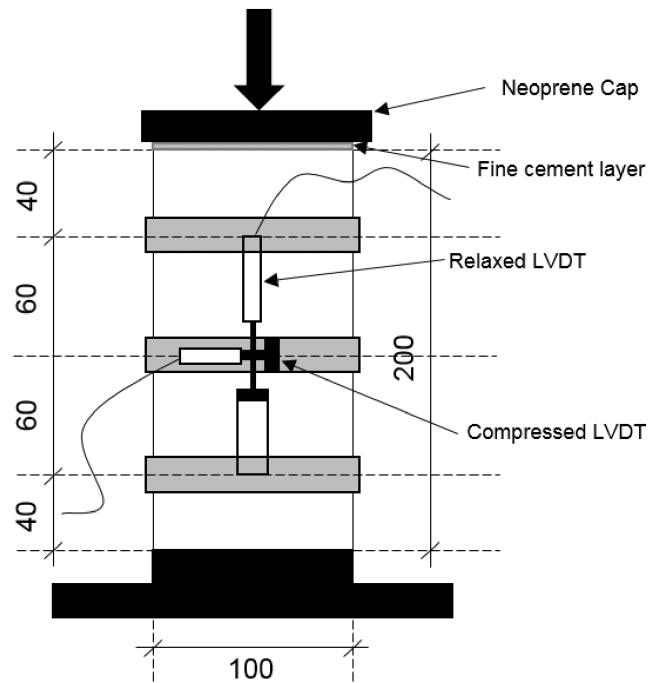


FIGURE 9 Instrumentation and test set-up for uniaxial compression cylinder test.

require safety equipment and experience in surface finishing. It should be noted that to ensure a nearly perfect contact between the loading platens and the top surface of the cylinders, a fine layer of cement not exceeding 5-mm thickness was mixed and applied on the top surface of the cylinders 2 days before testing to allow it to dry and gain a similar concrete strength (30–40 MPa). The purpose of this layer was to further cover any aggregates and fibers at the top surface of the cylinder, which could otherwise potentially cause damage to the neoprene cap and lead the load to be applied at an unfavorable angle resulting in premature failure. Hence, this fine cement layer ensured a better function of the neoprene pads, which resulted in better evaluation of the compressive σ - ε relationship, concrete strength f_{icm} , modulus of elasticity E_{icm} , and Poisson's ratio μ . A displacement-controlled loading rate of 1.2 mm/min was adopted as it was found to be the most suitable following trial tests to assess the effect of fibers on the brittle lightweight concrete and derive the full compressive σ - ε relationship.

4 | RESULTS AND DISCUSSION

4.1 | Workability

Slump tests according to BS EN 12390-2⁵⁹ were carried out immediately after mixing the concrete with the results reported in Table 4. For plain lightweight concrete, the mix proportion and specimen preparation

TABLE 4 Slump values for the mixes tested.

Mix	f_{ck} (MPa)	Properties		Slump (mm)		
		w/c	Fiber	Plain	$V_f = 1\%$	$V_f = 2\%$
1	30	0.47	3D	91	66	32
2	30	0.47	4D	98	49	26
3	35	0.41	3D	86	46	28
4	40	0.36	5D	88	42	20

techniques, detailed in Sections 3.2 and 3.3 of the present work, yielded satisfactory slump values and surface finishing of specimens. This agrees with previous work on plain LYTAG concrete.^{16,64} It can be seen that the addition of fibers drastically reduced workability. This was also observed by Swamy and Jojagha⁶⁵ who carried out workability tests on steel fiber-reinforced LYTAG concrete and Zeybek et al.⁴⁶ who carried out experimental investigations on concrete strengthened with recycled fibers from waste tires. At fiber dosage of $V_f = 2\%$, it was observed that the finishing process became challenging, the possibility for balling of fibers high, and inhomogeneity of concrete likely. This further emphasizes that for fibrous mixes, fiber dosage should not exceed $V_f = 1.5\%–2\%$ based on workability challenges if no superplasticizers or water reducing agents are used. Furthermore, this agrees with other researchers such as Düzgün et al.³⁹ who reported workability issues with $V_f > 1.5\%$. It also appears that the mixes having fibers with more extensive hooks held the slump together more tightly, which led to lower slump values than those mixes having fibers with less extensive hooks. It should be noted that the mixing and vibration time was increased as workability reduced owing to the increased need for compaction (this agrees with Düzgün et al.³⁹).

4.2 | Density

The average water-saturated density of the lightweight concrete produced was measured for each mix at 28 days after curing based on three cubes each with a width of 100 mm according to BS EN 12390-7.⁶⁵ Oven-dry density was also measured for plain LYTAG according to BS EN 12390-7.^{65,66} The water-saturated densities were in the range of 1900–2000 kg/m³, while the oven-dry densities were in the range of 1700–1780 kg/m³ for all specimens. The difference between densities of LWAC and SFRLC specimens appeared to be negligible, which may suggest the need of a better vibration technique and larger specimens to measure density to avoid potential size-effects with the usage of macro fibers. This agrees with several researchers.^{2,11,28,33,41,67,68}

4.3 | Crushing cube compressive strength

The mean compressive strength based on the crushing cube tests is shown in Table 5. The compressive strength values of fibrous cubes were identical or similar to those of plain cubes. Therefore, fiber reinforcement has little to no influence on the compressive strength of lightweight concrete. This observation was in line with Swamy et al.'s²⁶ findings who carried out compressive cube tests on fibrous LYTAG lightweight concrete. All failure patterns were satisfactory according to BS EN 12390-3.⁶⁹ This was the case since all cubes' side faces failed due to lateral tensile expansion with little damage to top and bottom faces of the cubes confined by the platens (Figure 10). As previously discussed, little to no effect of any types of fibers was seen on the crushing compressive strength of lightweight concrete; however, a longer duration of time was recorded for the cube load to drop to 80% of the peak load at which point the test was stopped. This observation implied an increased ductility of the fibrous lightweight concrete cubes. Upon releasing the crushing machine steel plates, it was apparent that the cubes had been storing energy throughout the test via steel fibers and abruptly moved as an initially compressed spring. Further inspection of fibrous specimens revealed that the fibers acted as lateral confining elements for the cubes by bridging the cracks thus preventing the load from dropping instantly as in the case of plain concrete. The effect of fibers on ductility is further inspected by studying the uniaxial compressive stress–strain behavior of cylinders.

4.4 | Uniaxial compressive properties

4.4.1 | Uniaxial σ – ϵ behavior

Figure 11 depicts the complete uniaxial stress–strain curves of cylinders under compression, with both axial and lateral strains measured (the latter demonstrating the confinement effect provided by the fibers as they bridge the cracks developing due to tension in the

TABLE 5 Average values from crushing cube tests based on three cubes per V_f .

Mix	Compressive strength (MPa)			$f_{lck,cube}^b$	Standard deviation	Coefficient of variation
	$f_{icm,cube}^a$					
	0%	1%	2%			
1	37	37 (0.0%)	38 (2.7%)	33	0.21	2.192
2	36	37 (2.8%)	34 (-5.6%)	33	0.68	1.902
3	45	42 (-6.7%)	44 (-2.2%)	38	0.91	2.645
4	50	49 (-2.0%)	51 (2.0%)	44	0.34	2.329

Note: The values between brackets show the percentage change in strength in each mix compared to the plain concrete control specimen.

^aAverage compressive strength from the test.

^bManufacturer's characteristic strength.

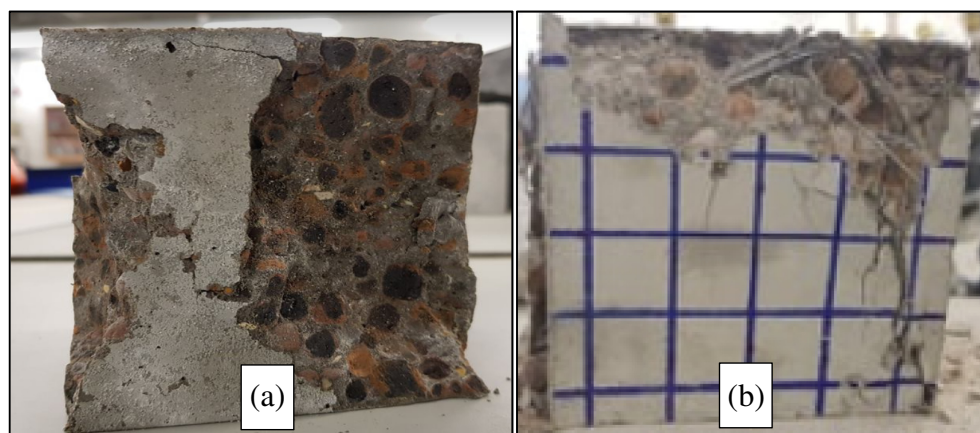


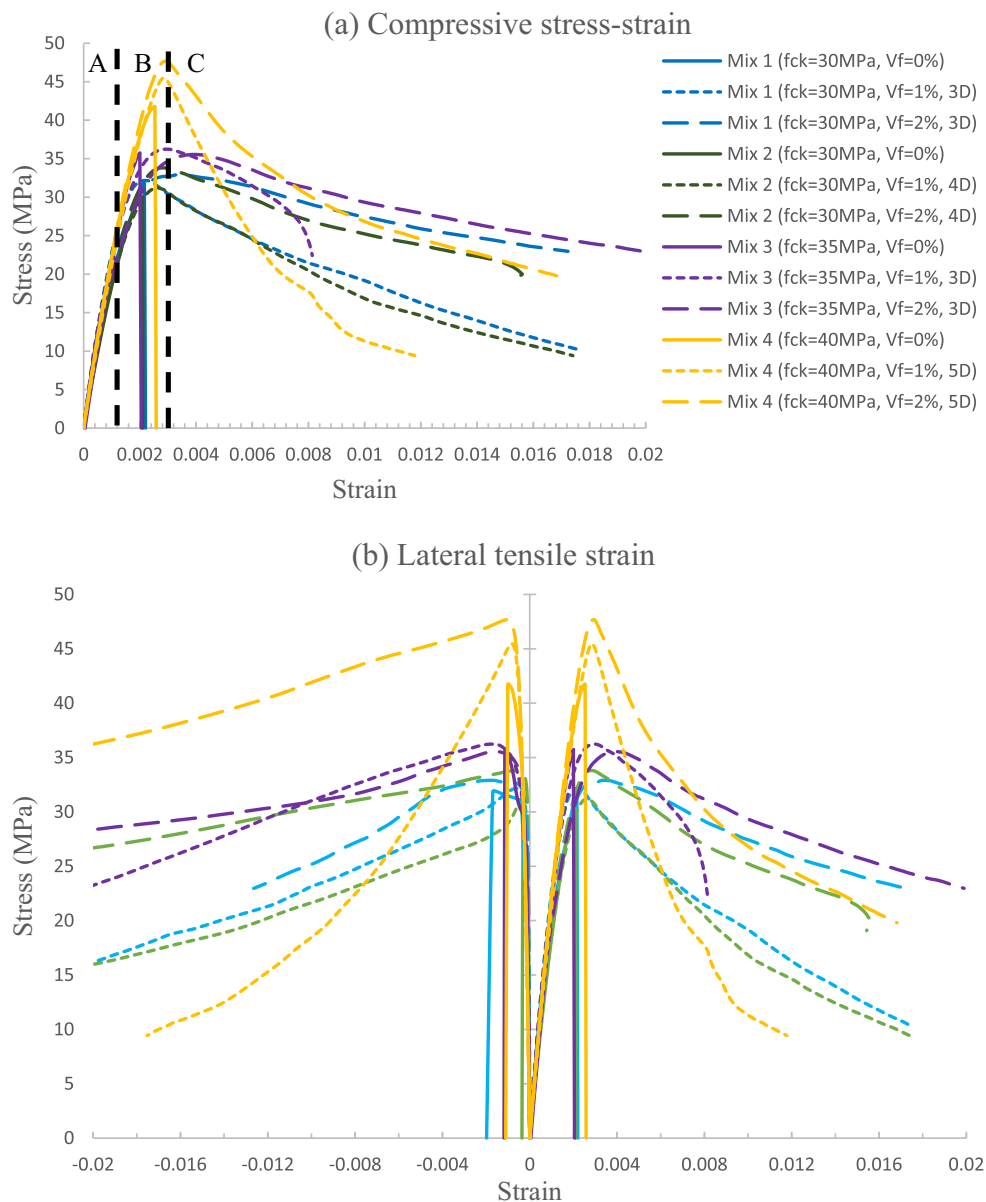
FIGURE 10 Satisfactory crushing failures of (a) LWAC cube and (b) SFRLC cube.

orthogonal direction to the axial compressive load). The curves clearly show the enhancements provided by the fibers in comparison to the plain concrete samples, which will be discussed in detail in the following sections. Unlike normal weight concrete, which remains largely linear up until 30%–45% of maximum load,⁷⁰ plain PFA lightweight concrete's stress–strain tested in this work remained linear up until 60%–70% of peak load with fibrous specimens having the least linearity due to steel fibers presence initiating micro cracking in the concrete. Domagala⁴² reported a stress–strain linearity of up to 90%–95% of the peak load for LWAC and 85% of the peak load for SFRLC specimens. The difference between the two results could be attributed to the more homogeneity of the lightweight concrete used in Domagala⁴² due to its smaller PFA coarse aggregates of 4–8 mm with water absorption of 25%, in comparison to the present work's PFA coarse aggregates of 4–14 mm with water absorption of 15%. Overall, the rough surface and porous coarse lightweight aggregates seem to enable a better bond with cement, which makes it act as a monolithic material prolonging the linear behavior in the ascending portion of the compressive stress–strain curve, which is the case in Domagala's work. It also causes it to fail in a brittle

pronounced manner once fracture develops due to the poor aggregate interlock mechanism, as also reported in Grabois et al.,²⁴ Kayali et al.,³⁰ and Domagala⁴² as the aggregates themselves are fractured through unlike normal-weight aggregates, which fracture at the interface with mortar. Similar behavior was reported in pumice concrete as coarse aggregates develop high bond with cement due to their rough surface and increased porosity and water absorption.^{21,33} Expanded clay concrete with lower water absorption and smoother aggregates is less homogenous, which causes earlier cracking and less monolithic behavior, leading to fibers influencing the modulus of elasticity more effectively.^{20,34}

The behavior of lightweight concrete can be split into three stages. During stage A, both LWAC and SFRLC cylinders experience a progressive linear load increase up to a load of 60%–70% of peak load corresponding to a strain of about 0.95‰, at which macro-cracking starts to take place in the middle section of the cylinder. This slightly reduces the secant modulus of elasticity and marks the start of stage B. As soon as a larger crack is formed, the cylinder specimens for plain lightweight concrete mixes collapse in a sudden manner (Figure 12a). This is attributed to the nature of lightweight aggregate, which

FIGURE 11 (a) Mean compressive uniaxial stress–strain curves and (b) lateral tensile strain (shown alongside the axial compressive strain).



was observed to be sheared through at failure. This behavior agrees with several researchers.^{24,30,42} For fibrous lightweight concrete, however, stage B initiates a plateau-like behavior, which lasts up to a strain of within the interval of 2.5–3.2‰ depending on the fiber dosage. The higher the V_f , the larger the strain at peak. The macro cracking at the end of stage A initiated by the presence of fibers leads to the activation of fiber-bridging mechanism preventing the formation of a larger shear crack at stage B. Furthermore, this causes redistribution of stresses via energy dissipation of multiple cracks unlike in the case of plain lightweight concrete. At stage C, as extensive lateral cracking dominates the post-peak behavior of the cylinders, the compressive load finally begins to decline in a ductile manner for the fibrous mixes.

It is interesting to note that upon inspection of cracking in the tested cylinder specimens, it was apparent that the cracks ran parallel to the direction of loading causing eventual splitting of the LWAC cylinders (as can be seen in Figure 12a), while a network of interconnected cracks being bridged by steel fibers was a typical cracking pattern of SFRLC cylinders (as shown in Figure 12b). Domagala⁴² also reported similar cracking paths, although some instances where fibers failed to bridge cracks were reported. The latter was not observed in the current work probably due to the higher V_f dosages used (1% and 2%) as compared to Domagala's work where the highest V_f was 0.8%.⁴² Since none of the fibers were seen to rupture or break during the compression tests, the different maximum tensile strength of 3D, 4D, and 5D fibers was never reached, and thus did not take part in the behavior of

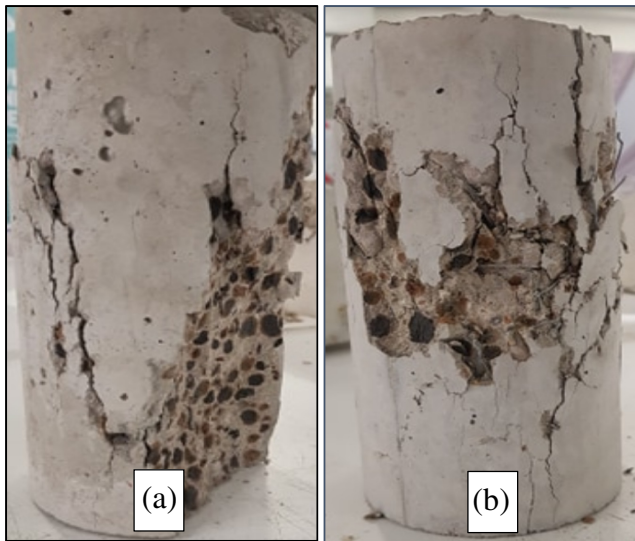


FIGURE 12 Typical crack patterns at failure of (a) plain cylinder and (b) fibrous cylinder LWAC.

SFRLC specimens. Hence, provided that fibers are normally activated following cracking, it is safe to assume that the extensive hooks or bends are only responsible for bridging the crack during phase B and providing a lateral confinement to the cylinder, which prevents the expansion of tensile cracking, therefore increasing the compressive strength. While 3D fibers with the basic mechanical hook (single bend) end up being pulled out more easily, 4D (double bend) and 5D (triple bend) fibers bond better to the brittle lightweight concrete increasing confinement and thus upgrading LWAC peak compressive strength.

4.4.2 | Elastic properties in compression

For LWAC and SFRLC specimens, Young's modulus of elasticity was calculated to be an average of 20.1, 19.7, 20.1, and 22.1 GPa for mixes 1, 2, 3, and 4, respectively, with no noticeable difference between LWAC and SFRLC specimens of the same mix (as can be seen in Figure 13). Kayali et al.³⁰ who carried out compression tests on high strength fibrous and plain lightweight concrete also reported a trivial influence on the modulus of elasticity as steel fibers were added, while Domagala⁴² who carried out compression tests on plain and fibrous PFA concrete reported a similar trend in results as this work's for cubic and cylindrical compressive strengths and modulus of elasticity. These values remain somewhat lower than Eurocode 2 provisions,⁶⁹ which suggest 22.1, 22.8, and 23.4 GPa for LC30, LC35, and LC40, respectively. SFRLC cylinders did not exhibit a tangible variation in the elastic values of neither the modulus of elasticity nor Poisson's ratio from the plain concrete cylinders.

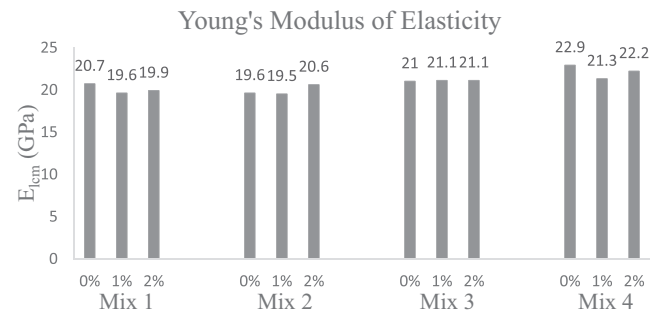


FIGURE 13 Measured modulus of elasticity values for the four mixes tested.

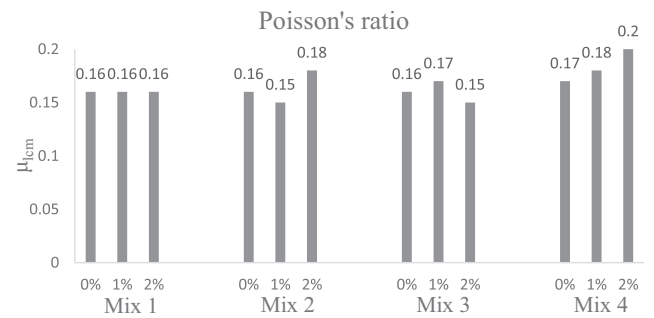


FIGURE 14 Measured Poisson's ratio values for the four mixes tested.

The measured Poisson's ratio values ranged between 0.15 and 0.20 for all LWAC and SFRLC specimens (Figure 14). These were also consistent with findings reported by Lambert who carried compression tests on plain PFA lightweight concrete.¹⁶ Therefore, modulus of elasticity and Poisson's ratio remained unaffected with the addition of hooked-end fibers to the lightweight concrete mix, whereas post-peak ductility substantially increased. This finding is consistent with work by Li et al. in which random hooked-end fibers in SFRC were found to have little to no effect on the modulus of elasticity, while slight favorable or unfavorable effect of fiber reinforcement on compressive strength can be seen.⁷¹

4.4.3 | Cylinder compressive strength

From Figure 15, it is observed that (compared to 3D fibers), 4D and 5D fibers with extensive hooks were capable of further increasing the mean compressive strength of the cylinders regardless of the plain concrete's strength. On the other hand, there is an insignificant change in the compressive strength 3D fibers were used. The compressive strength for plain concrete of Mix 2 was increased by 5% and 12.2% when 4D fibers were added to LC30 with dosages of $V_f = 1\%$ and 2% , respectively.

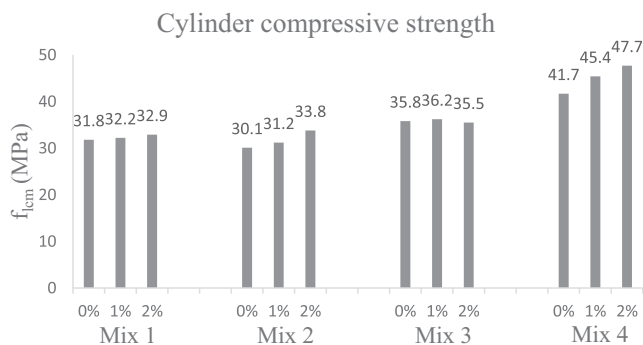


FIGURE 15 Measured cylinder compressive strengths for the four mixes tested.

Similarly, for Mix 4, the compressive strength for plain concrete was increased by 7.8% and 15% when 5D fibers were incorporated in the LC40 mix with dosages of $V_f = 1\%$ and 2% , respectively. As reported earlier in Section 4.3 of the present study, the SFRLC *cube* compressive crushing strength was found to have no practical difference to that of LWAC counterparts. Nevertheless, there was a slight apparent increase in SFRLC *cylinder* compressive strength compared to that of corresponding LWAC samples. This can be attributed to the size effect of cylinder specimens in comparison to the length of fibers and the casting direction to loading direction, which is perpendicular for cubic specimens and parallel for cylindrical specimens. The latter's casting-loading arrangement is known to encourage favorable alignment of steel fibers to arrest cracks more efficiently. This concept was also discussed by Domagala.⁴²

4.4.4 | Compression toughness

The compression toughness was chosen to evaluate the energy absorption and post-peak ductility of SFRLC in compression. Similar to Liu et al.² who based their estimation of compression toughness on ASTM C 1018⁷² approach, the compression toughness was calculated by dividing the total area up to a strain three times larger than the peak strain by the area up to the peak strain, under the compression σ - ϵ curve. Since plain lightweight concrete failed once compression peak was reached, the toughness was 1 for these specimens. Despite the little increase in compressive strength, especially for 3D fibers, the ductility was significantly enhanced by more than 2.5 times for $V_f = 1\%$ and close to three times for $V_f = 2\%$ (as depicted in Figure 16). It is interesting to see that the compressive toughness calculated for different concrete strengths with identical fiber reinforcement differed. While it is clear that the random distribution of fibers play an important factor in the latter,

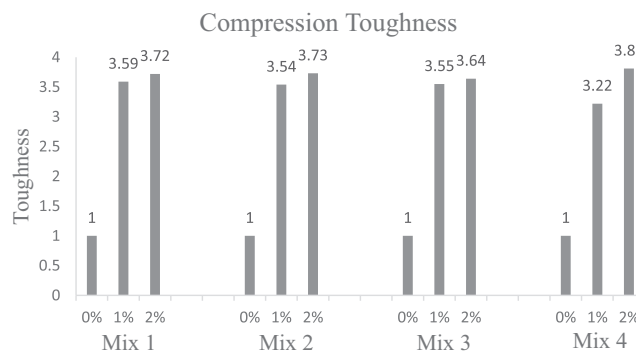


FIGURE 16 Calculated compression toughness for the four mixes tested.

it is well established that the stronger the mix, the more brittle the concrete, which in turn lowers ductility.^{30,73,74}

This is confirmed by the compression tests carried out. For instance, Mix 4 with the highest compressive strength $f_{ck} = 40$ MPa reinforced with the triple bend 5D fibers provided the lowest compressive toughness when $V_f = 1\%$ of all the cylinders of the same V_f . However, for the same mix, when $V_f = 2\%$ of 5D fibers were added to plain lightweight concrete cylinders, the increase in compression toughness was 18% higher than that of $V_f = 1\%$, which is the highest increase amongst all the cylinders tested. The latter comes as no surprise since 5D fibers were expected to offer more lateral confinement than the rest of the fibers, especially while having a stronger bond strength due to being mixed with stronger concrete. 4D and 3D fibers led to 4% and 6% increase in compression toughness, respectively, when V_f was increased from 1% to 2%. Since the compression toughness was increased by an average of 260% by adding fiber dosage of $V_f = 1\%$ and a slight further increase with $V_f = 2\%$, it was concluded that the benefit of fiber reinforcement on compressive ductility is perhaps optimized at $V_f = 1\%$, with more benefit being reported with the highly brittle stronger concrete grades.

5 | COMPRESSIVE σ - ϵ CONSTITUTIVE MODEL AND VALIDATION

5.1 | Relationship between cylinder f_{lcm} and cube $f_{lcm,cube}$ strengths

Due to the difference in confinement and slenderness, a higher compressive strength was calculated for cubes $f_{lcm,cube}$ than cylinders f_{lcm} . Comparing the results from both plain and fibrous cylinders and cubes, the following relationship can be derived using linear regression analysis (with strengths measured in MPa) with $R^2 = 0.94$:

$$f_{lcm} = 1.75f_{lcm,cube}^{0.80} \quad (1)$$

One equation was deemed sufficient for both plain and fibrous PFA aggregate concrete as there was practically no difference in the compressive strength due to fibers, as discussed earlier. Based on table 11.3.1 from Eurocode 2⁷⁰ $f_{lcm} = (f_{lcm,cube} - 10)/1.1 + 8$. The Eurocode equation overestimates the mean cylinder strength by over 10% for stronger mixes with an overall average of ~6% overestimation, while the proposed equation predicts the mixes' mean cylinder strength reasonably well with an average underestimation of ~1%.

5.2 | Static modulus of elasticity

Modulus of elasticity appears to be connected to concrete compressive strength. This is also supported by Eurocodes and *fib* models.^{70,75} Based on linear regression analysis for both plain and fibrous lightweight concrete (with the modulus of elasticity measured in GPa), the following equation was derived to link E_{lcm} to f_{lcm} with $R^2 = 0.96$.

$$E_{lcm} = 4.55f_{lcm}^{0.42} \quad (2)$$

As observed from the compressive tests, it should be borne in mind that fibers have practically no effect on the elastic behavior of lightweight concrete. However as previously discussed, if the aggregate–cement bond is weak, the contribution of fibers can take place early on during loading due to fibers crack initiation, thus affecting the modulus of elasticity in a positive or a negative

manner depending on fiber dosage and type. These lightweight aggregates are thought to be less rough or smooth with a lower water absorption. A comparison between the ratios of the predicted-to-experimental values of the moduli of elasticity can be found in Table 6. This is based on a total of 36 plain and fibrous cylinders tested in the present experimental investigations as well as using the most relevant equations derived by previous researchers.

As expected, Lambert's equation based on plain LYTAG predicted E_{lcm} with good accuracy. Slate et al.,⁷⁸ ACI318-89,⁷⁹ and Liu et al.² equations, which take into consideration the density of concrete, also predict E_{lcm} of this work's tested specimens with high accuracy. Eurocode 2⁶³ overestimates E_{lcm} , while the rest of the models appear to underestimate E_{lcm} .

To check the validity of Equations (1) and (2) using experimental data established outside this work, the predictions of the proposed equations were compared with the results of these experiments as shown in Table 7. It should be noted that in some instances where only crushing cube strength was given, Equation (1) was used to derive f_{lcm} , which was in turn input in Equation (2) to finally calculate E_{lcm} (for instance: in the work of Liu et al.² where no compressive testing of cylinder was carried out). Overall, the regression power Equation (2) suggested was successful at predicting E_{lcm} values for lightweight concrete of different lightweight aggregate types (such as expanded clay, expanded shale, pumice, PFA), different cement strengths (i.e., 42.5 and 52.5 MPa), plain compressive cube strengths (ranging from 19.5 MPa¹⁶ to 87 MPa²⁰), fiber types (hooked end, crimped, opposite end), fiber materials (plastic, carbon, steel) and fiber volume fractions (ranging from 0.25% to

Researcher	Equation	$E_{lcm}(Eq)/E_{lcm}(Exp)$
Lambert (1982) ¹⁶	$E_{lcm} = 5.82f_{lcm,cube}^{0.32}$	0.88–0.95 (0.90)
Shah and Ahmad (1985) ⁷⁶	$E_{lcm} = 0.036\rho^{1.5}\sqrt{f_{lcm}}$	0.78–0.84 (0.80)
BS 8110 (1985) ⁷⁷	$E_{lcm} = (0.2f_{lcm,cube} + 20) \cdot (\rho/2400)^2$	0.79–0.84 (0.81)
Slate et al. (1986) ⁷⁸	$E_{lcm} = (3320\sqrt{f_{lcm}} + 6895) \cdot (\rho/2320)^{1.5}$	0.88–0.93 (0.90)
ACI 318-89 (1989) ⁷⁹	$E_{lcm} = 0.043\rho^{1.5}\sqrt{f_{lcm}}$	0.94–1.00 (0.98)
Zhang and Gjørsv (1991) ⁷⁴	$E_{lcm} = 1190f_{lcm,cube}^{0.67}$	0.64–0.72 (0.67)
Eurocode 2 (1992) ⁸⁰	$E_{lcm} = 9500(\rho/2400)^2 \cdot f_{lcm}^{0.33}$	0.86–0.90 (0.87)
Eurocode 2 (2004) ⁷⁰	$E_{lcm} = 22(f_{lcm}/10)^{0.33} \cdot \eta_E$	1.07–1.12 (1.10)
Lo et al. (2016) ¹⁷	$E_{lcm} = 4.33f_{lcm,cube}^{0.37}$	0.79–0.84 (0.80)
Liu et al. (2019) ²	$E_{lcm} = 5681.67f_{lcm}^{0.403} \cdot (\rho/2250)^{1.146}$	0.90–0.93 (0.92)
Proposed model (Equation 2)	$E_{lcm} = 4.55f_{lcm}^{0.42}$	0.94–0.99 (0.96)

Note: Average values shown between brackets.

TABLE 6 Prediction of E_{lcm} of LWAC and SFRLC values based on 36 cylinder specimens tested in this work, using proposed and previous models.

TABLE 7 Validation of E_{lcm} values for both LWAC and SFRLC predicted using the proposed Equations (1) and (2) against the experimental data established by other researchers.

Researcher	Coarse aggregate			Specimen	$E_{lcm(Eqt)}/E_{lcm(Exp)}$
	Type	Surface	Water absorption (%)		
Lambert (1982) ¹⁶	PFA	Rough	15	Plain	0.99–1.02 (1.01)
Swamy et al. (1993) ²⁶	PFA	Rough	13	Plain	1.02–1.06 (1.04)
				SFRLC	0.99–1.02 (0.97)
Gao et al. (1997) ²⁰	Expanded Clay	Rough	10	Plain	1.02–1.03 (1.03)
				SFRLC	0.93–1.02 (0.97)
Kayali et al. (2003) ³⁰	PFA	Rough	–	Plain	1.08–1.09 (1.08)
				SFRLC	1.22–1.23 (1.22)
				PFRLC ^a	1.07–1.19 (1.15)
Domagala (2011) ⁴²	PFA	Rough	25	Plain	0.93–1.02 (0.98)
				SFRLC	0.92–1.03 (0.97)
Grabois et al. (2016) ²⁴	Expanded Clay	Rough	9.1	Plain	0.94–0.96 (0.95)
				SFRLC	0.96–1.00 (0.98)
Zhao et al. ^b (2018) ³²	Expanded Shale	Rough	–	Plain	0.96–1.03 (0.99)
				SFRLC	0.97–1.10 (1.04)
Badogiannis et al. (2019) ³³	Pumice + Gravel	Rough	22	Plain	0.86–0.87 (0.86)
				SFRLC	0.90–1.00 (0.94)
				PFRLC	0.98–1.00 (0.99)
Liu et al. (2019) ²	Shale ceramiste	Smooth	2.2	Plain	0.95–0.95 (0.95)
				CFRLC ^c	1.16–1.32 (1.24)
				SFRLC	1.12–1.35 (1.25)
Total Mean					1.03

Note: Average values shown between brackets.

^aPlastic fiber-reinforced LWAC.

^bMedium strength and high strength cements are used.

^cCarbon fiber-reinforced LWAC.

2%). Equation 2 slightly overestimated E_{lcm} of SFRLC specimens with aggregates that were smooth, had low water absorption, or developed too many air voids due to poor compaction.³⁰

5.3 | Poisson's ratio

Similar to the findings reported by Lambert,¹⁶ Poisson's ratio appeared to be random between 0.15 and 0.20 (as can be seen in Figure 14). No particular relation linking Poisson's ratio to concrete strength, modulus of elasticity, fiber type, and dosage was formulated (although the general trend of both axial and lateral strains can be seen in Figure 11b). This behavior is identical to that of plain lightweight concrete and stems from the fact that fibers have no impact on the elastic behavior of lightweight concrete as discussed previously. In order for Poisson's ratio to be altered for fibrous concrete materials,

fibers have to intervene earlier to provide either confinement to change the lateral strain or reinforcement similar to vertical rebars to change the axial strain. This does not occur until cracking has developed at stage B, as explained earlier in Section 4.4.1 of the present study.

5.4 | Fiber-reinforcing factor ρ_f

Several researchers defined the fiber factor (or fiber-reinforcing index $V_f[L_f/d_f]$ where L_f is the fiber length and d_f is fiber diameter), as a parameter to evaluate the performance of fibrous concrete or to derive material properties in tension, flexure, and compression.^{20,81–85} Although, this factor was used to develop empirical and semi-empirical equations for fibers of different shapes and material properties in the past, it has some shortcomings due to its generic and simplistic nature. For example, with regards to the hooked-end steel fibers used in this

work, the fiber-reinforcing index does not quantify the effect of the different extensive mechanical hooks or bends on the properties of concrete. So, if a hooked-end fiber and a straight fiber shared identical aspect ratio L_f/d_f , the fiber-reinforcing index would be identical for both fibers. This translates to both fibers influencing the mechanical properties of a similar concrete in the same way, which is not accurate since the mechanical hooks in bent fibers enhance the mechanical properties of brittle concrete more than straight fibers. Khuntia et al.⁸⁶ defined a shape factor β to adjust the fiber-reinforcing index based on their geometry as follows $V_f(L_f/d_f) \beta$, with $\beta = 1, 2/3$, and $3/4$ for SFRC with hooked-end or crimped steel fibers, plain, or round steel fibers and SFRLC with hooked-end or crimped steel fibers, respectively.⁸⁶ While the latter equation is considered to be more comprehensive in comparison with the classical fiber reinforcing index, it does not take into consideration the geometrical and mechanical differences within the same fiber group such as the case between hooked-end 3D and 5D hooks, which enable the latter to display an improved performance under loading. Besides, it does not distinguish between fibers of different materials. For instance, plastic fibers and carbon fibers, which are usually straight and come in filaments exhibit bond strengths with concrete different to that of steel fibers. Hence, a new fiber-reinforcing factor is proposed in the present research work to quantify the improvement in the behavior of SFRLC both in tension (in related experimental work) and compression, while considering different fiber types, geometries, aspect ratios, and materials; as expressed in Equation 3.

$$\rho_f = V_f(L_f + L_e)/d_f(\delta \cdot \kappa) \quad (3)$$

where V_f is the fiber volume fraction (%), L_f is the fiber length, L_e is the effective fiber length, d_f is fiber diameter, δ is the shape factor, and κ is the material factor. The shape factor δ is taken as 0.8 for straight fibers, 0.9 for crimped fibers, 1 for single hooked-end fibers (or fibers with $n_b = 1$, such as 3D), 1.5 for double hooked-end fiber (or fibers with $n_b = 2$, such as 4D), and 2 for triple hooked-end fiber (or fibers with $n_b = 3$, such as 5D) with n_b as the number of bends. The shape factors are chosen based on the maximum possible strength that can be developed from pull-out studies on DRAMIX 3D, 4D, and 5D fibers found in this work and also by Abdallah et al.^{54,55,85,87} who used similar fibers in their study. The material factor κ is 1 for steel, 0.3 for plastic, and 0.1 for carbon fibers. These were based on comparison of the literature followed by inverse analysis. The effective fiber length L_e is defined as the length required to develop the maximum pull-out strength of fiber based on pull-out

TABLE 8 Fiber reinforcing factor and fiber reinforcing index for the fibers used in this work.

Fiber type	Proposed fiber reinforcing factor ρ_f	Conventional fiber reinforcing index $V_f(L_f/d_f)$
3D	0.773	0.667
4D	1.220	0.667
5D	1.657	0.667

tests, which are detailed elsewhere, with preliminary study found in Al-Naimi and Abbas.⁵⁸ L_e is calculated from the following expression:

$$L_e = L_h + 5d_f \quad (4)$$

where L_h is the fiber hook length for hooked-end fibers. L_h is taken as 0 for both crimped and straight fibers. The fiber-reinforcing factor ρ_f , which is a way to quantify the fiber–matrix interfacial bond, was used in the present work to derive the SFRLC uniaxial compressive σ – ϵ relationship. The fiber-reinforcing factors and fiber-reinforcing index with $V_f = 1\%$ for the different hooked-end fibers used in this work are summarized in Table 8. The second column in Table 8 refers to the *proposed* modified reinforcing factor and it is demonstrating the allowance for the number of fiber bends (unlike the last column showing the *conventional* factor, which remain unchanged for different fiber number of bends).

Table 8 shows that, unlike the proposed fiber-reinforcing factor ρ_f , the conventional fiber-reinforcing index is incapable of assessing the effect of increasing the number of bends between 3D, 4D, and 5D on concrete. For this reason, ρ_f appears to be a better estimate for quantifying the effect of fiber reinforcement on concrete. Thus, the fiber factor ρ_f will be incorporated into material equations to derive a σ – ϵ constitutive model compressive using the experimental results of LWAC and SFRLC specimens tested in this work as well as those tested in previous research.

5.5 | Proposed constitutive compressive σ – ϵ model

The proposed compressive stress–strain model is depicted in Figure 17. For the tested LWAC specimens, the strain at peak load ϵ_{1c1} was equal to the strain at ultimate load ϵ_{1cu} since concrete failed in a sudden brittle manner once it reached the peak strength. This also agrees with several researchers^{24,42} and Eurocode 2.⁷⁰ This is the case because once the load has reached its peak strength, the

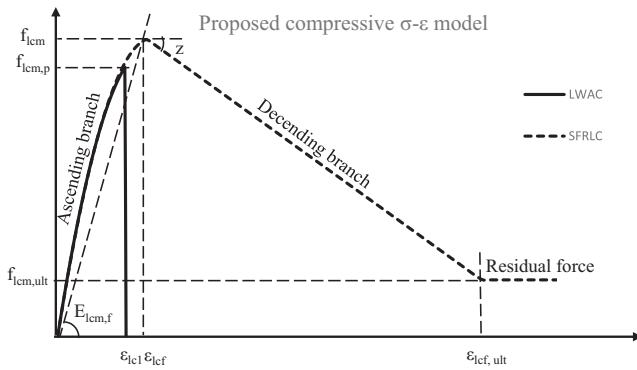


FIGURE 17 Proposed σ - ϵ relationship for plain and fibrous lightweight concrete.

lightweight aggregates end up being sheared through providing no resistance against cracking unlike in the case for normal weight aggregate concrete. Using the results from the uniaxial compressive cylinder tests, the strain at peak of plain lightweight concrete can be written as:

$$\epsilon_{lc1} = 0.87/1000 f_{lcm,p}^{0.28} \quad (5)$$

where $f_{lcm,p}$ is the peak mean cylinder compressive strength of plain lightweight concrete.

For SFRLC specimens, however, the strain at peak strength and at ultimate strength were seen to be influenced by concrete strength and fiber-matrix interfacial bond, which is affected by fiber type, geometry, and dosage. Using regression analysis, the maximum concrete cylinder strength for both LWAC and SFRLC can be calculated using the following proposed expression:

$$f_{lcm} = f_{lcm,p} (1 + 0.08 \rho_f^{0.33}) \quad (6)$$

where ρ_f is the fiber-reinforcing factor discussed earlier in the previous section.

Figure 18 shows the influence of fiber reinforcement on compressive strength of LWAC using Equation (6). It can be seen that when $\rho_f < 0.3$ (corresponding to $V_f = 0.4\%$ for 3D fibers), the influence of fibers on the compressive strength is trivial. The limit is shown herein using ρ_f rather than V_f to take into consideration the fiber shape, material, type, and geometry. Furthermore, to calculate the strain at peak of SFRLC with E_{lcm} (MPa) calculated from Equation (2):

$$\epsilon_{lcf} = \epsilon_{lc1} + 6.67 \sqrt{\rho_f} / E_{lcm} \quad (7)$$

This equation takes into account the increased brittleness when concrete strength grade is higher and so it

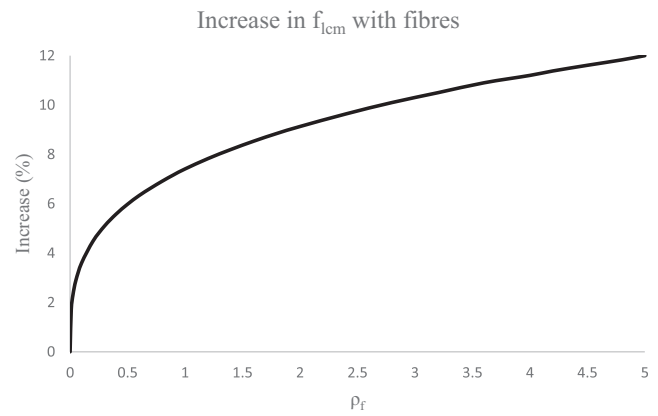


FIGURE 18 Percentage increase of compressive strength with the addition of fibers as function of the fiber reinforcing factor ρ_f .

adds a realistic concept of compression toughness and ductility. Adopting a second-order equation form, commonly used by several researchers such as Soroushian and Lee,⁸⁸ the complete compressive stress-strain for lightweight concrete can be derived from:

$$f_{lc} = \min \left[f_{lcm} \left(\alpha \left(\frac{\epsilon_{lc}}{\epsilon_{lcf}} \right) - (\alpha - 1) \left(\frac{\epsilon_{lc}}{\epsilon_{lcf}} \right)^2 \right), f_{lcm} \right] \text{ for } \epsilon_{lc} \leq \epsilon_{lcf} \quad (8)$$

$$f_{lc} = z(\epsilon_{lc} - \epsilon_{lcf}) + f_{lcm} \geq f_{lcm,ult} \text{ for } \epsilon_{lc1,f} < \epsilon_{lc} < \epsilon_{lcf,ult} \quad (9)$$

$$f_{lc} = f_{lcm,ult} \text{ for } \epsilon_{lc} = \epsilon_{lcf,ult} \quad (10)$$

Equation (8) for the calculation of the ascending part of the compressive stress-strain relationship, includes the definition of a plateau when $f_{lc} = f_{lcm}$ depending on the value of factor α (Equation 11), which is based on the composite material peak elastic modulus calculated from $E_{lcm,f} = f_{lcm} / \epsilon_{lcf}$ and the base composite material peak elastic modulus $E_{b,f}$:

$$\alpha = E_{b,f} / E_{lcm,f} + 0.11 \quad (11)$$

$E_{b,f}$ is a constant that was empirically determined from the uniaxial cylinder compression tests in the present study and found to be equal to 21,150 MPa.

The slope of the descending branch z in Equation (9) can be determined from the following equation:

$$z = -190 f_{lcm} (1 - 0.33 \rho_f^{0.5}) \leq 0 \quad (12)$$

$f_{lcm,ult}$ in Equation (10) is the ultimate residual post-peak axial compressive stress calculated using the following regression analysis equation:

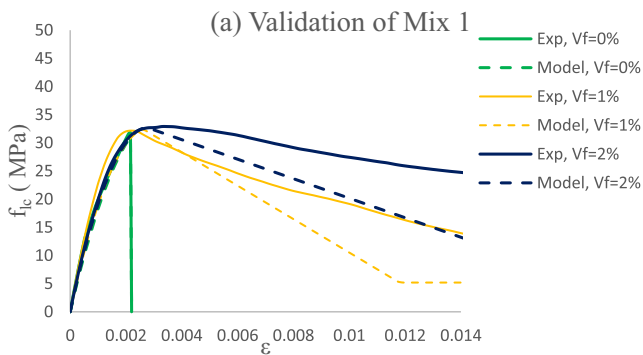


FIGURE 19 Predicted versus experimental uniaxial compression σ - ϵ curves of Mix 1.

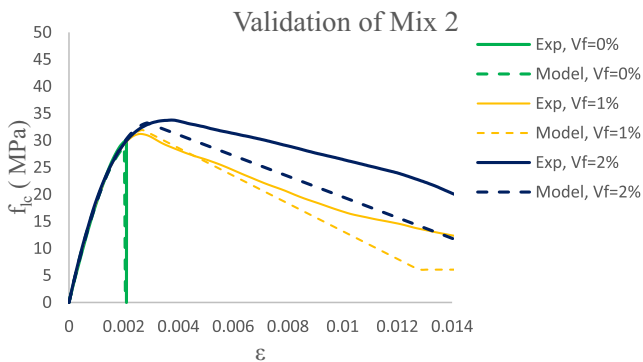


FIGURE 20 Predicted versus experimental uniaxial compression σ - ϵ curves of Mix 2.

$$f_{lcm,ult} = 2.1\rho_f + 0.11f_{lcm} \quad (13)$$

5.6 | Validation of the proposed constitutive compressive σ - ϵ model

Figures 19–22 illustrate the comparisons between the experimental and predicted compressive stress–strain curves from mixes of different strengths, V_f , and fiber types up to a strain of 0.014. Although generally conservative during the post-peak, the suggested model is seen to be successful at predicting the compressive strength and strain at peak. The predicted stress values remained accurate at all strain levels, while that of the peak compressive strength was predicted within 96% for all the tested specimens.

To further verify the adequacy of the proposed compressive stress–strain model for plain and fibrous lightweight concrete, the results of uniaxial compression tests on LWAC and SFRLC cylinders reported by Domagala⁴² were predicted using compression models of other researchers^{2,69,88,89} as well as the proposed compression model derived in the present study (and depicted in Figure 17) and the results are shown in Figures 23 and

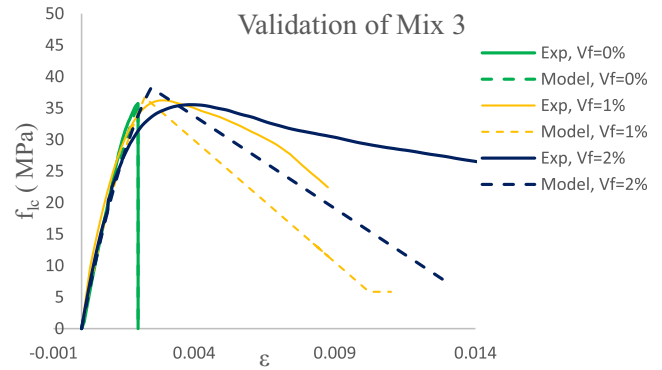


FIGURE 21 Predicted versus experimental uniaxial compression σ - ϵ curves of Mix 3.

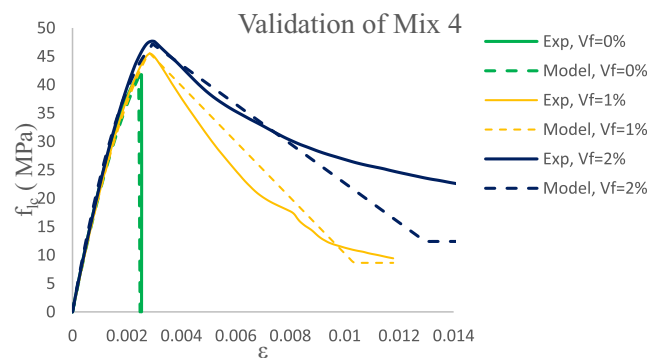


FIGURE 22 Predicted versus experimental uniaxial compression σ - ϵ curves of Mix 4.

24. It should be borne in mind that currently there is a scarcity in the compression stress–strain data for SFRLC, which prompted the current experimental research study. Besides, some existing data reported a decrease rather than an increase in compressive strength with fiber addition stemmed from poor bond (such as the case of plastic fiber) and poor compaction or mixing and thus they were not considered in the validation exercise.³⁰

Figures 23 and 24 show that the proposed model accurately predicted the modulus of elasticity (within 2% for both LWAC and SFRLC), peak compressive strengths (1% overestimation for LWAC and 5% underestimation for SFRLC), strains at peak (1% overestimation for LWAC and 3.5% underestimated for SFRLC) and post-peak ductility with good accuracy for both plain and fibrous cylinders in consideration. It should be noted that Eurocode 2⁶³ prediction clearly overestimated the modulus of elasticity and underestimated the strain at peak for LWAC. This is due to Eurocode 2 assumption for strain at peak of LWAC being lower than that of normal weight concrete. Such assumption has been shown to be inaccurate throughout the experimental tests of this work and others since the lower modulus of elasticity for LWAC results in

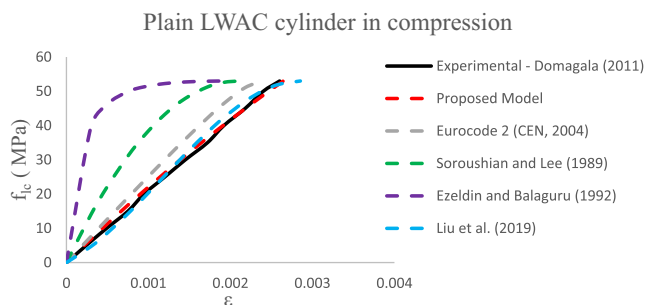


FIGURE 23 Prediction of LWAC compressive behavior with $V_f = 0\%$.⁴²

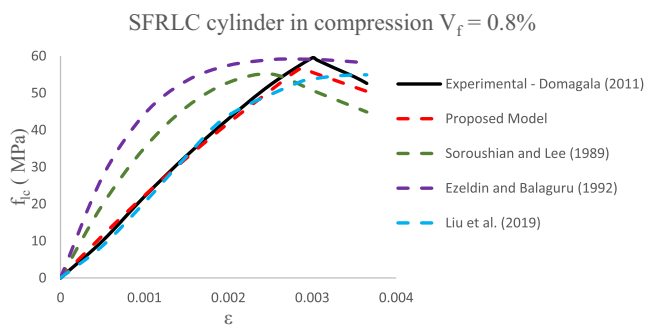


FIGURE 24 Prediction of SFRLC compressive behavior with $V_f = 0.8\%$.⁴²

having a higher strain at peak than NWC for similar strengths. Liu et al.² also confirmed the latter based on 842 tests of plain and fibrous lightweight concrete cylinders. While Soroushian and Lee⁸⁸ and Ezeldin and Balaguru⁸⁹ stress-strain models seem to be more suitable for plain and fibrous normal weight concrete since they highly overestimated the modulus of elasticity for LWAC and SFRLC, Liu et al.² model prediction for plain and fibrous lightweight concrete is considered reasonable. Liu et al.² model predicted the modulus of elasticity within 1% for both SFRLC and LWAC, slightly underestimated the peak strength of SFRLC by 7% and overestimated the strain at peak of LWAC by 8%. Nonetheless, the strain at peak for SFRLC was overestimated by 20% and as a result, the ductility was overestimated. This is the case because unlike the proposed model, Liu et al.² model does not allow for the increased brittleness associated with higher concrete strength grades and simply an additional strain is derived based on the fiber-reinforcing index. This was also noticed in the rest of the models examined in the comparison where a factor of the fiber-reinforcing index is added linearly to SFRLC concrete strength. This was proven to be too simplistic in this work, since the proposed constitutive model derives the peak compressive strengths and strains for fibrous concrete, while considering the improved fiber-matrix interfacial

bond as well as the increased brittleness, as the concrete grade becomes higher. Based on the preceding discussion, the proposed compressive σ - ϵ for LWAC and SFRLC models are regarded as a viable and accurate predicting tool for the compressive behavior of plain and fibrous lightweight concretes with various concrete strengths, fiber types, geometries, and fiber volume fractions.

6 | CONCLUSIONS AND RECOMMENDATIONS FOR FUTURE WORK

In the present research work, experimental studies were carried out to examine the uniaxial compressive behavior of recycled lightweight aggregate concrete reinforced with single and multiple-bend steel fibers. Consequently, the following conclusions and recommendations were made:

- A unique generic constitutive compressive stress-strain model capable of predicting accurately the behavior of SFRLC composites was proposed. Due to the nature of the constitutive model and its related equations that depend mainly on fiber-reinforcing factor ρ_f and plain concrete compressive strength, the model is deemed flexible and adaptable to other fibrous composites.
- The proposed model's predicted pre-peak stress values remained accurate at all strain levels with the compressive strength being predicted within 96% for all the tested specimens, whilst the post-peak predictions were slightly conservative. Using a case study of LWAC and SFRLC, it was found that the proposed constitutive model is more reliable than some of the most established fibrous concrete models available in the literature.
- In the present study, a new fiber-reinforcing factor ρ_f is proposed, which is affected by concrete compressive strength, number of fiber bends, and fiber volume fraction. Due to this versatility and taking into account all the key parameters affecting the fiber-concrete interaction, the new fiber-reinforcing factor is considered to be more accurate and representative compared to the somewhat simplistic volume fraction V_f usually used.
- The uniaxial compressive behavior of fibrous concrete was found to be proportional to the fiber-reinforcing factor.
- Due to the absence of an aggregate interlock mechanism, it was confirmed that LWAC, which acts as a monolithic material, fails in a brittle sudden manner once the peak strength is reached, due to the shearing through the coarse lightweight aggregate. This pronounced brittleness was the key reason for introducing

fibers to provide ductility. The effect of the incorporation of fiber reinforcement on lightweight concrete in compression was found to be more pronounced with the increase in plain concrete compressive strength, number of fiber bends, and fiber volume fraction.

- The addition of fibers to lightweight concrete was found to add compressive strength as the number of bends n_b and fiber volume fraction V_f were increased. The increase in peak compressive strength was insignificant for specimens with 3D fibers; however, those with 4D and 5D fibers exhibited an increase of up to 15% moving from $V_f = 0\%$ to $V_f = 2\%$. This behavior is attributed to the capability of multiple hook fibers to bend more efficiently and provide confinement to the concrete specimens tested.
- The compression toughness used to quantify ductility was found to increase as V_f was increased. The compression toughness of plain lightweight concrete was increased by an average of 260% upon adding fiber dosage of 1% for all fiber types. A further insignificant increase of compression toughness of 5% on average was recorded at $V_f = 2\%$ as compared to $V_f = 1\%$ for both 3D and 4D specimens, while that of 5D specimens was increased by about 18%.
- No practical effect on Poisson's ratio was found with the addition of fibers to the lightweight concrete mix, which was measured to be between 0.15 and 0.20. This was also the case for modulus of elasticity, which remained constant up to approximately 70% of peak strength.
- Regression equations linking cube and cylinder compressive strengths, and static modulus of elasticity for both plain and fibrous lightweight concrete were derived based on the experimental program detailed in the present research work. These equations were also validated and were preceded by an examination of a vast literature of SFRLC, which included different lightweight aggregate types, cement strengths, plain concrete compressive strengths, fiber types, fiber materials, and fiber volume fractions. The compression behavior proposed model main characteristics can serve to enrich codes and guidelines of plain and fibrous lightweight concrete.
- While negligible influence of fibers was reported on density, workability of LWAC was found to be negatively affected by the addition of fibers especially with multiple-bend fibers (for example 5D) and at high fiber dosages such as $V_f > 1\%$. To address the latter issue, it is recommended that the lightweight concrete's coarse aggregates are mixed after achieving the SSD state with sand being fully oven-dried. Furthermore, the use of superplasticizers is recommended for mixes with $V_f > 1\%$ as that will enhance the mixing process and

mitigate risks of having voids and non-homogeneity in the mix. Another recommendation to enhance workability and avoid size effects would be to use bigger sections such 150 mm³ cubes rather than 100 mm³.

Recommendations for future work are also made below.

- Further studies describing the stress–strain behavior of PFA lightweight fibrous concrete in compression. These should also serve to further validate the work in the present paper.
- Validation of the constitutive models suggested in this paper using finite element analysis especially for different fiber types, volumes, and materials.
- Carrying out experiments on both the material and structural levels on multiple bend fibers (described here as 4D and 5D fibers).
- Using the fiber factor to investigate the effect of fibers on the tensile and shear behavior of lightweight concrete.

NOTATIONS

f _{ck} , cube	characteristic cube compressive stress
f _{ck} , flc	characteristic cylinder compressive stress
f _{lc}	cylinder compressive stress
f _{cm}	mean cylinder compressive stress
f _{cm} , p	mean cylinder compressive stress of plain concrete
f _{cm} , cube	mean cube compressive stress
E _{lcm}	mean value of Young's modulus of elasticity
n _b	number of bends
d _f	diameter of fiber
L _e	effective fiber anchorage length
L _E	embedded length of fiber
κ	fiber material factor
ρ _f	fiber reinforcing factor
δ	fiber shape factor
V _f	fiber volume fraction
L _f	length of fiber
E _{lcm} , f	peak elastic modulus of SFRLC
μ _{lc}	Poisson's ratio
ε	strain
ε _{lc1}	strain at peak compressive stress of LWAC
ε _{lc f}	strain at peak compressive stress of SFRLC
ε _{t1}	strain at post-cracking first residual tensile stress
ε _{lcu}	strain at ultimate compressive stress of LWAC
ε _{lc f, ult}	strain at ultimate compressive stress of SFRLC

σ	stress
σ_y	Fiber yield stress
σ_u	Fiber ultimate stress
Ef	Young's modulus of elasticity fiber
SFRLC	Steel fiber-reinforced lightweight concrete
LWAC	Lightweight aggregate concrete

DATA AVAILABILITY STATEMENT

The data that support the findings of this study are available from the corresponding author upon reasonable request.

ORCID

Ali A. Abbas  <https://orcid.org/0000-0002-0114-4511>

REFERENCES

- Al-Khaiat H, Haque MN. Effect of initial curing on early strength and physical properties of lightweight concrete. *Cem Concr Res*. 1998;28:859–66.
- Liu X, Wu T, Liu Y. Stress–strain relationship for plain and fibre-reinforced lightweight aggregate concrete. *Construct Build Mater*. 2019;225:256–72.
- Chandra S, Berntsson L. *Lightweight aggregate concrete science. Technology and Applications*. Delhi, India: Standard Publishers Distributors; 2003 ISBN 81-8014-052-0.
- Ahn YB, Jang JG, Lee HK. Mechanical properties of lightweight concrete made with coal ashes after exposure to elevated temperatures. *Cement Concrete Comp*. 2016;72:27–38.
- Gerritse A. Design considerations for reinforced lightweight concrete. *Int J Cem Compos Lightweight Concr*. 1981;3(1):57–69.
- LYTAG. Technical manual. London: LYTAG Ltd; 2011.
- LYTAG. Ramboll frame comparison study. 2014 [cited 2019 Dec 31]. Available from: <https://www.aggregate.com/our-businesses/LYTAG>
- Libre NA, Shekarchi M, Mahoutian M, Soroushian P. Mechanical properties of hybrid fiber reinforced lightweight aggregate concrete made with natural pumice. *Construct Build Mater*. 2011;25(5):2458–64.
- Campione G. Flexural and shear resistance of steel fiber-reinforced lightweight concrete beams. *J Struct Eng*. 2014; 140(4):1–8.
- Dias-da-Costa D, Carmo RNF, Graça-e-Costa R, Valença J, Alfaiate J. Longitudinal reinforcement ratio in lightweight aggregate concrete beams. *Eng Struct*. 2014;81:219–29.
- Mo KM, Goh S, Alengaram U, Visintin P, Jumaat M. Mechanical, toughness, bond and durability-related properties of lightweight concrete reinforced with steel fibres. *Mater Struct*. 2017; 50(1):46.
- Lim HS, Wee TH, Mansur MA, Hau KK. Flexural behavior of reinforced lightweight aggregate concrete beams. Asia-Pacific structural engineering and construction conference. Kuala Lumpur: APSEC; 2006. p. 68–82.
- Chen H, Huang C, Tang C. Dynamic properties of lightweight concrete beams made by sedimentary lightweight aggregate. *J Mater Civil Eng*. 2010;22(6):599–606.
- Wu C, Kan Y, Huang C, Yen T, Chen L. Flexural behavior and size effect of full scale reinforced lightweight concrete beam. *J Mar Sci Technol*. 2011;19(2):132–40.
- Badogiannis E, Kotsovos M. Monotonic and cyclic flexural tests on lightweight aggregate concrete beams. *Earthq Struct*. 2014; 6(3):317–34.
- Lambert G. Properties and behaviour of structural lightweight (LYTAG—sand) concrete. PhD thesis, University of Sheffield. 1982.
- Lo TY, Cui H, Memon SA, Noguchi T. Manufacturing of sintered lightweight aggregate using high-carbon fly ash and its effect on the mechanical properties and microstructure of concrete. *J Clean Prod*. 2016;112:753–62.
- Bilodeau A, Kodur V, Hoff G. Optimization of the type and amount of polypropylene fibres for preventing the spalling of lightweight concrete subjected to hydrocarbon fire. *Cem Concr Compos*. 2004;26(2):163–74.
- Collins R, Sherwood P. Use of waste and recycled materials as aggregates. London: H.M.S.O.; 1995.
- Gao J, Sun W, Morino K. Mechanical properties of steel fiber-reinforced, high-strength, lightweight concrete. *Cem Concr Compos*. 1997;19(4):307–13.
- Campione G, La Mendola L. Behavior in compression of lightweight fiber reinforced concrete confined with transverse steel reinforcement. *Cem Concr Compos*. 2004;26(6):645–56.
- Abbas AA, Syed Mohsin SM, Cotsovos DM. Seismic response of steel fibre reinforced concrete beam–column joints. *Eng Struct*. 2014;59:261–83.
- Di Prisco M, Colombo M, Dozio D. Fibre-reinforced concrete in fib model code 2010: principles, models and test validation. *Struct Concr*. 2013;14(4):342–61.
- Grabois TM, Cordeiro GC, Filho RDT. Fresh and hardened-state properties of self-compacting lightweight concrete reinforced with steel fibers. *Construct Build Mater*. 2016;104: 284–92.
- Ritchie A, Kayali O. The effects of fiber reinforcement on lightweight aggregate concrete. In: Neville A, editor. *Proceedings of RILEM symposium on fiber reinforced cement and concrete*. London: The Construction Press Ltd; 1975. p. 247–56.
- Swamy N, Jones R, Chiam A. Influence of steel fibers on the shear resistance of lightweight concrete I-beams. *ACI Struct J*. 1993;90(1):103–14.
- Kang T, Kim W. Shear strength of steel fiber-reinforced lightweight concrete beams. Oklahoma: Korea Concrete Institute; 2010. p. 1386–92.
- Iqbal S, Ali A, Holschemacher K, Bier T. Mechanical properties of steel fiber reinforced high strength lightweight self-compacting concrete (SHLSCC). *Construct Build Mater*. 2015;98:325–33.
- IEA. *World energy outlook 2019*. 2019 [cited 2020 Oct 1] Available from: <https://www.iea.org/reports/world-energy-outlook-2019/coal#abstract>
- Kayali O, Haque M, Zhu B. Some characteristics of high strength fiber reinforced lightweight aggregate concrete. *Cem Concr Compos*. 2003;25(2):207–13.
- Mo KM, Yap KKQ, Alengaram UJ, Jumaat MZ. The effect of steel fibres on the enhancement of flexural and compressive toughness and fracture characteristics of oil palm shell concrete. *Construct Build Mater*. 2014;55:20–8.
- Zhao M, Zhao M, Chen M, Li J, Law D. An experimental study on strength and toughness of steel fiber reinforced expanded-shale lightweight concrete. *Construct Build Mater*. 2018;183: 493–501.

33. Badogiannis EG, Christidis KI, Tzanetatos GE. Evaluation of the mechanical behavior of pumice lightweight concrete reinforced with steel and polypropylene fibers. *Construct Build Mater.* 2019;196:443–56.
34. Campione G, Miraglia N, Papia M. Mechanical properties of steel fibre reinforced lightweight concrete with pumice stone or expanded clay aggregates. *Mater Struct.* 2001;34(4):201–10.
35. Balaguru P, Dipsia MG. Properties of fiber reinforced high-strength Semilightweight concrete. *ACI Mater J.* 1993;90(5):399–405.
36. Balaguru P, Foden A. Properties of fiber reinforced structural lightweight concrete. *ACI Struct J.* 1996;93(1):62–78.
37. Hassanpour M, Shafiq HP, Mahmud H. Mechanical properties of structural lightweight aggregate concrete containing low volume steel fiber. *Arabian J Sci Eng.* 2014;39(5):3579–90.
38. Ali A, Iqbal S, Holschemacher K, Bier TA. Comparison of flexural performance of lightweight fibre-reinforced concrete and normal weight fiber-reinforced concrete. *Period Polytech Civ Eng.* 2017;61(3):498–504.
39. Düzgün O, Gül R, Aydın A. Effect of steel fibers on the mechanical properties of natural lightweight aggregate concrete. *Mater Lett.* 2005;59(27):3357–63.
40. Guneyisi E, Gesoglu M, Ozturan T, Ipek S. Fracture behavior and mechanical properties of concrete with artificial lightweight aggregate and steel fiber. *Construct Build Mater.* 2015;84:156–68.
41. Balendran R, Zhou F, Nadeem A, Leung A. Influence of steel fibres on strength and ductility of normal and lightweight high strength concrete. *Build Environ.* 2002;37(12):1361–7.
42. Domagala L. Modification of properties of structural lightweight concrete with steel fibres. *J Civ Eng Manag.* 2011;17:36–44.
43. Karalar M, Özkılıç Y, Deifalla A, Aksoyulu C, Arslan M, Ahmad M, et al. Improvement in bending performance of reinforced concrete beams produced with waste lathe scraps. *Sustainability.* 2022;14(19):12660.
44. Elik A, Özkılıç Y, Zeybek Ö, Özdöner N, Tayeh B. Performance assessment of fiber-reinforced concrete produced with waste lathe fibers. *Sustainability.* 2022;14:11817.
45. Kalpana M, Tayu A. Light weight steel fibre reinforced concrete: a review. *Mater Today Proc.* 2020;22(3):884–6.
46. Zeybek Ö, Özkılıç Y, Çelik A, Deifalla A, Ahmad M, Sabri M. Performance evaluation of fiber-reinforced concrete produced with steel fibers extracted from waste tire. *Front Mater.* 2022;9:1057128.
47. Dehghani A, Aslani F. Effect of 3D, 4D, and 5D hooked-end type and loading rate on the pull-out performance of shape memory alloy fibres embedded in cementitious composites. *Construct Build Mater.* 2021;273:121742.
48. Guler S, Funda Z. Residual strength and toughness properties of 3D, 4D and 5D steel fiber-reinforced concrete exposed to high temperatures. *Construct Build Mater.* 2022;327:126945.
49. Mohamed A, Tayeh B, Abu Aisheh Y, Salih M. Exploring the performance of steel fiber reinforced lightweight concrete: a case study review. *Case Stud Constr Mater.* 2023;18:e01968.
50. Comité Européen De Normalisation. Cement. Composition, specifications and conformity criteria for common cements. London: British Standard; 2011 BS EN 197-1.
51. Comité Européen De Normalisation. Methods of testing cement. Determination of strength. London: British Standard; 2016 BS EN 196-1.
52. Comité Européen De Normalisation. Aggregates for concrete. London: British Standard; 2013 BS EN 12620.
53. Bekaert. [cited 2023 May 12]. 2020 Available from: <<https://www.bekaert.com/en/>>
54. Abdallah S, Rees DWA, Hamidreza S, Fan M. Understanding the effects of hooked-end steel fibre geometry on the uniaxial tensile behaviour of self-compacting concrete. *Construct Build Mater.* 2018;178:484–94.
55. Abdallah S, Fan M, Zhou X. Effect of hooked-end steel Fibres geometry on pull-out behaviour of ultra-high performance concrete. *Int J Civ Environ Struct Constr Archit Eng.* 2016;10(12):1594–9.
56. Comité Européen De Normalisation. Tests for mechanical and physical properties of aggregates, part 6: determination of particle density and water absorption. London: British Standard; 2013 BS EN 1097-6.
57. Evangelista ACJ, Tam VWY. Properties of high-strength lightweight concrete using manufactured aggregate. *Proc Inst Civ Eng Constr Mater.* 2018;173:157–69. <https://doi.org/10.1680/jcoma.17.00082>
58. Al-Naimi H, Abbas A. Ductility of steel-fibre-reinforced recycled lightweight concrete. *COMPdyn 2019: 7th international conference on computational methods in structural dynamics and earthquake engineering*, 24–26 Jun 2019. Crete, Greece: Institute of Structural Analysis and Antiseismic Research; 2019. p. 4009–23. <https://doi.org/10.7712/120119.7203.19035>
59. Comité Européen De Normalisation. Testing fresh concrete. Slump test. London: British Standard; 2009 BS EN 12390-2.
60. ASTM C39/C39M-20. Standard test method for compressive strength of cylindrical concrete specimens. West Conshohocken, PA: ASTM International; 2020 www.astm.org
61. ASTM C469/C469M-14. Standard test method for static modulus of elasticity and Poisson's ratio of concrete in compression. West Conshohocken, PA: ASTM International; 2014 www.astm.org
62. ASTM C1231/C1231M-15. Standard practice for use of Unbonded caps in determination of compressive strength of hardened cylindrical concrete specimens. West Conshohocken, PA: ASTM International; 2015 www.astm.org
63. Crouch LK, Pearson JB. Neoprene capping for static modulus of elasticity testing. *ACI Mater J.* 1996;92(6):1–6.
64. Swamy RN, Lambert GH. Mix design and properties of concrete made from PFA coarse aggregates and sand. *Int J Cem Compos Lightweight Concr.* 1983;3(4):263–75.
65. Swamy R, Jojagha A. Workability of steel fibre reinforced lightweight aggregate concrete. *Int J Cem Compos Lightweight Concr.* 1982;4(2):103–9.
66. Comité Européen De Normalisation. Testing hardened concrete. Density of hardened concrete. London: British Standard; 2019 BS EN 12390-7.
67. Wang JY, Chia KS, Liew JYR, Zhang MH. Flexural performance of fiberreinforced ultra lightweight cement composites with low fiber content. *Cement Concr Compos.* 2013;43:39–47. <https://doi.org/10.1016/j.cemconcomp.2013.06.006>
68. Daneti SB, Wee TH. Behavior of hybrid fiber reinforced high strength lightweight aggregate concrete. *Mag Concr Res.* 2011; 63(1):785–96.
69. Comité Européen De Normalisation. Testing hardened concrete. Compressive strength of test specimens. London: British Standard; 2019 BS EN 12390-3.
70. Comité Européen De Normalisation. Eurocode 2: design of concrete structures—part 1: general rules and rules for buildings. London: British Standard; 2004 BS EN 1992-1-1.

71. Li F-Y, Cao C-Y, Cui Y-X, Wu P-F. Experimental study of the basic mechanical properties of directionally distributed steel fibre-reinforced concrete. *Adv Mater Sci Eng*. 2018;3:1–11.
72. ASTM C1018. Standard test method for flexural toughness and first-crack strength of fiber-reinforced concrete (using beam with third-point loading) (Withdrawn 2006). West Conshohocken, PA: ASTM International; 1997 www.astm.org
73. Gettu R, Bazant ZP, Karr ME. Fracture properties and brittleness of high-strength concrete. *ACI Mater J*. 1990;87:608–17.
74. Zhang MH, Gjorv OE. Mechanical properties of high-strength lightweight concrete. *ACI Mater J*. 1991;88(3):240–7.
75. Fédération Internationale du béton. fib model code for concrete structures 2010. Berlin: Ernst and Sohn; 2013. p. 147–50.
76. Shah SP, Ahmad SH. Structural properties of high strength concrete and its application for prestressed concrete. *J Prestressed Concr Inst*. 1985;30(6):92–119.
77. BS 8110. Structural use of concrete: part—I: code of practice for design and construction. London: British Standards Institution; 1985.
78. Slate FO, Nilson AH, Martinez S. Mechanical properties of high-strength lightweight concrete. *Journal of American Concrete Institute*. 1986;83(4):606–13.
79. ACI. Building code requirements for structural concrete. Farmington Hills, MI: ACI; 1989.
80. CEN (European Committee for Standardisation). EN 1992-1-1: Eurocode 2: design of concrete structures—part 1. General rules for buildings. Brussels, Belgium: CEN; 1992.
81. Lok T-S, Xiao JR. (1999): flexural strength assessment of steel fiber reinforced concrete. *J Mater Civ Eng*. 1999;11(3):188–96.
82. Ou YC, Tsai MS, Liu KY, Chang KC. Compressive behaviour of steel fiber reinforced concrete with a high reinforcing index. *J Mater Civ Eng*. 2012;24(2):207–15.
83. Liao W-C, Perceka W, Liu E-J. Compressive stress-strain relationship of high strength steel fiber reinforced concrete. *J Adv Concrete Technol*. 2015;13:379–92.
84. Kwan AKH, Chu SH. Direct tension behaviour of steel fibre reinforced concrete measured by a new test method. *Eng Struct*. 2018;176:324–36.
85. Abdallah S, Fan M, Rees DWA. Analysis and modelling of mechanical anchorage of 4D/5D hooked end steel fibres. *Mater Des*. 2016;112:539–52.
86. Khuntia M, Stojadinovic B, Goel SC. Shear strength of normal and high-strength fiber reinforced concrete beams without stirrups. *ACI Struct J*. 1999;96(2):282–9.
87. Abdallah S, Fan M, Zhou X. Pull-out behaviour of hooked end steel Fibres embedded in ultra-high performance mortar with various W/B ratios. *Int J Concr Struct Mater*. 2017;11(2):301–13.
88. Soroushian P, Lee C. Constitutive modeling of steel fiber reinforced concrete under direct tensile and compression. In: Swamy RN, Barr B, editors. *Fiber reinforced cement and concrete—recent developments*. Cardiff: University of Wales College of Cardiff; 1989. p. 363–77.
89. Ezeldin AS, Balaguru PN. Normal and high strength fiber reinforced concrete under compression. *J Mater Civ Eng*. 1992;4(4): 415–29.

AUTHOR BIOGRAPHIES



Hasanain K. Al-Naimi, Doctoral Graduate, University of East London, London, UK. Email: hasanainalnaimireal@gmail.com.



Ali A. Abbas, Associate Professor of Structural Engineering, University of East London, London, UK. Email: abbas@uel.ac.uk.

How to cite this article: Al-Naimi HK, Abbas AA. Constitutive model for plain and fiber-reinforced lightweight concrete under compression. *Structural Concrete*. 2023;24(6): 7625–47. <https://doi.org/10.1002/suco.202200646>